An Analysis of the Xenon Enhanced Computed Tomography Technique for Measuring Regional Cerebral Blood Flow

by

Keith Stewart St Lawrence

A thesis presented to the University of Manitoba

in partial fulfillment of the requirements

for the degree of M.Sc. in Physics

May, 1991.

ISBN 0-315-77028-7

AN ANALYSIS OF THE XENON ENHANCED COMPUTED TOMOGRAPHY TECHNIQUE FOR MEASURING REGIONAL CEREBRAL BLOOD FLOW

BY

KEITH STEWART ST. LAWRENCE

A thesis submitted to the Faculty of Graduate Studies of the University of Manitoba in partial fulfillment of the requirements of the degree of

MASTER OF SCIENCE

Table of Contents

Acknowledgements

First and foremost, I would like to acknowledge my supervisor Dr. Peter Dunscombe for his guidance and advise. Secondly, I would like to thank Dr. Jeff Bews for his incredible patience for being able to withstand my constant badgering and questioning. The advice of Dr. Walter Huda and Dr. Ting Lee also proved to be invaluable.

I would like to thank the National Science and Engineering Research Council for their financial support during the two years of my M.Sc. studies.

On a personal note, I would like to thank my family and friends for their support. In particular, I wish to thank my old communication pal Krista Thomas, although I do not believe she will every realize how much her support meant to me. Finally, I wish to thank my parents for having the good sense to have me in the first place.

ABSTRACT

Xenon enhanced computed tomography (XeCT) is a non-invasive technique for measuring regional cerebral blood flow (rCBF). Two aspects of XeCT were studied in this thesis. First of all, the precision of XeCT was compared to another technique for measuring rCBF and secondly, a proposed simplification to the clinical application of XeCT was investigated.

XeCT was compared to the $C^{15}O_2$ buildup/dynamic positron emission tomography rCBF measuring technique ($C^{15}0_2$PET). $C^{15}0_2$PET was chosen for this comparison because of the similarities between it and XeCT and because $C^{15}0_2$PET is based on PET (the imaging modality generally considered the best for measuring cerebral blood flow). The two techniques were compared by studying the effect statistical noise, which is present in the serial images collected during the application of both techniques, has on their precision. This comparison was carried out using Monte Carlo type computer simulations and the results of the simulations indicated that XeCT is actually more precise than $C^{15}O_2$PET. This finding was attributed to the better signal to noise ratio in the images obtained by the former.

The XeCT technique requires that the arterial concentration of xenon be measured continuously during a patient study. The arterial concentration of xenon is usually measured indirectly by monitoring the concentration of xenon in end-tidal expired air with a thermoconductivity analyzer (the two concentrations are assumed in equilibrium). An alternative method was

proposed, which utilizes the CT scanner to measure the expired air concentration. In this method, referred to as expired air scanning, the patient's expired air is channelled through the scan field using a flexible plastic tube and sampled by the CT scanner in conjunction with monitoring the uptake of xenon in cerebral tissue. This new method simplifies XeCT by eliminating the need for a specialized instrument for measuring the expired air concentration. The viability of expired air scanning was analyzed using phantom studies and computer simulations. The results of the phantom studies demonstrated that the CT scanner does in fact have the capability to detect changes in the xenon concentration in air. The computer simulations showed that although expired air scanning will introduce error into rCBF measurements, this error is quite small compared to one of the dominant sources of error associated with XeCT: the statistical noise in the head images.

List of Figures

List of Tables

Chapter 1

Overview

Over the latter half of this century many techniques have been developed for measuring regional cerebral blood flow (rCBF) in man. One such technique is xenon enhanced computed tomography (XeCT) and it is the focus of investigation of this thesis. In particular, two aspects of this technique are investigated. First, it is generally assumed that the gold standard for measuring rCBF is Positron Emission Tomography (PET) [Kety, 85]. To assess the potential of xenon enhanced CT as an alternative, the XeCT technique was compared, using computer simulations, to a PET based rCBF measuring technique. Second, a proposed modification to the XeCT technique, designed to simplify its application, was investigated using computer simulations and experimental measurements.

1.1 Clinical Applications of Regional Cerebral Blood Flow Measurements

The human brain represents only about two percent of the total body weight yet receives fourteen percent of the cardiac output and is responsible for twenty-three percent of the total body oxygen consumption [McHenry, 78]. Due to the brain's dependence on blood flow there is a great deal of clinical interest in measuring cerebral blood flow under normal and various pathological conditions.

One of the major applications of rCBF measurement is in the area of cerebral ischemia [Deshmukh, 78; McHenry, 78; Rescigno et al, 88]. It has been estimated that if rCBF falls below 20 ml/100g/min, some degree of permanent

neurologic deficit can be expected. However, if rCBF is maintained above 25 ml/100g/min the prognosis for recovery is reasonably good. rCBF measurements could therefore prove useful for evaluating the extent of recovery of a patient who has suffered cerebral ischemia due to a neurological disorder such as cerebrovascular disease, head trauma, or brain lesion.

rCBF measurements could also be used to evaluate the usefulness of, and the risks associated with, certain neurosurgical procedures such as by-pass surgery in cerebrovascular disease or the surgical repair of an intracranial aneurysm [Deshmukh, 78; Rescigno et al, 88]. Such neurosurgical procedures often require a cerebral artery to be clamped resulting in temporary regional ischemia.

The measurement of rCBF has been shown to be useful for diagnosing different types of headaches [Deshmukh, 78; Rescigno et al, 88]. Migraines, for instance, are associated with hemodynamic changes.

Research has been on going to determine the relationship between rCBF and degenerative diseases such as Alzheimer's disease and Parkinson's syndrome, as well as the relationship between rCBF and psychiatric disorders such as schizophrenia and depression [Deshmukh, 78; Rescigno et al, 88]. It is hoped that knowledge of rCBF during different stages of these diseases could aid in their management.

rCBF measurements could prove useful in understanding the therapeutic response of cerebral tumours to different treatments [Ott, 89; Lammertsma et al,

85]. If the blood flow to the tumour is low, then treatments such as chemotherapy and radiotherapy may prove less effective (chemotherapy is dependent on blood flow to deliver the drugs to the tumour [Shapiro et al, 86] while radiotherapy requires well-oxygenated tumours cells for treatments to be successful [Nelson et al, 86]).

These constitute but a few examples of the current uses of rCBF measurements. With more advanced techniques for measuring rCBF presently being developed, many additional clinical application will be possible.

1.2 Techniques for the Measurement of regional Cerebral Blood Flow

Most modern techniques for measuring rCBF are based on kinetic models which require the administration of a tracer followed by the measurement of its concentration in arterial blood and cerebral tissue. The simplest model used for this purpose is the single compartmental Kety model which describes the uptake or clearance of a nonmetabolized diffusible tracer in tissue [Kety, 51]. In this section, a brief historical outline of the many different Kety based rCBF techniques is presented.

The first successful technique for measuring blood flow based on the Kety model was the N_2O method [Kety et al, 48]. This technique uses the stable gas N_2O as the tracer. As it is impossible to measure the concentration of N_2O in cerebral tissue directly, the venous blood concentration, which is assumed to be in equilibrium with the tissue concentration, is measured. As a result of not

being able to measure the tissue concentration directly, this technique can only be used to measure global blood flow, and not the blood flow in specific volumes of cerebral tissue (ie. rCBF).

rCBF measurements became possible with the application of radioactive tracers. The concentration of a radioactive tracer in cerebral tissue can be determined using radiation detectors (gamma cameras) placed against the patient's head. 85-Kr was the first radioactive tracer used to measure rCBF in man [Lassen et al, 54; 64]. It was later replaced by 133-Xe, which proved to be a more satisfactory tracer due to the higher energy of its emitted photons [Obrist et al, 67; Hoedt-Rasmussen et al, 66]. However, gamma cameras are planar imaging devices and as such, a three dimensional activity distribution is superimposed onto two dimensions. Blood flow measurements using gamma cameras are applicable only to large volumes on the head, not specific volumes of cerebral tissue and any localized abnormalities in CBF will be difficult to detect. This superposition problem can only be solved by using tomographic imaging modalities.

rCBF measurements have been made with almost all of the tomographic imaging modalities: single photon emission computed tomography (SPECT), positron emission computed tomography (PET), transmission computed tomography (CT), with the exception of magnetic resonance imaging (MRI).

SPECT generates transverse images of the spatial distribution of photon emitting radionuclides and has been used in the application of the Kety model to

measure the concentration of a radioactive tracer in cerebral tissue [Lassen et al, 68; Celsis et al, 81; Lassen et al, 85]. There are two basic detector arrangements for SPECT scanners: a rotating gamma camera or an array of detectors surrounding the patient. The rotating gamma camera requires considerably more time than an array of detectors to acquire sufficient number of photons to produce suitable images for quantitative measurements. Therefore, the former is used less often in the application of the Kety model. The most common radioactive tracer for measuring rCBF with SPECT has been 133-Xe.

Serious disadvantages with SPECT include its poor spatial resolution and its susceptibility to scattered radiation [Lassen et al, 85]. The poor spatial resolution of SPECT puts a lower limit on the volume of cerebral tissue for which blood flow can be calculated, while scatter radiation will adversely effect the precision and accuracy of measurements. Other radionuclides such as ^{127}Xe and ^{123}I have photons of higher energy than ^{133}Xe and they have been suggested as alternative tracers, in an effort to reduce the effect of scattered radiation. A new class of tracers, called "chemical microspheres" have also been developed for measuring rCBF with SPECT [Rescigno et al, 88]. They have a prolonged retention in tissue and as a result, conventional slow rotational gamma cameras can be used. However, the kinetic models used to describe the deposition and retention of chemical microspheres in tissue can be complicated.

CT, which produces transverse images of the differential absorption of X-rays [Webb, 88; Barrett and Swindell, 81], has also been used in the application

of the Kety model [Kelcz et al, 78; Drayer et al, 80]. With this technique, the stable gas xenon, which is a contrast agent, is used as the diffusible tracer. As the concentration of xenon in tissue increases, there is a subsequent enhancement (increase) in CT number. CT scanning therefore provides a means of measuring the cerebral tissue concentration of xenon required by the Kety equation.

The major advantage of this technique is the excellent spatial and temporal resolution of the CT scanner. Due to the rapid acquisition time associated with CT, it is possible to completely characterize the washin or washout of xenon in cerebral tissue with dynamic scanning. This complete characterization in turn, makes possible the simultaneous measurement of blood flow and the blood/brain partition coefficient. The partition coefficient is defined as the ratio of the concentration of a substance in tissue to its concentration in blood at equilibrium and is a measure of tracer solubility [Kety, 51]. As will be discussed in Chapter 2.2, the Kety model requires prior knowledge of the partition coefficient to calculate rCBF. Most applications of the Kety model are unable to determine the partition coefficient simultaneous with rCBF and therefore the former must be estimated. If the correct value is not chosen, then the derived value of rCBF can be erroneous. By determining the partition coefficient and rCBF simultaneously, the XeCT technique offers the advantage of eliminating this potential source of error. Characterizing the washin/washout of the tracer with SPECT is not possible because of the poor temporal resolution of this modality.

PET yields transverse images of the distribution of an administered

positron emitting radionuclide by coincidence detection of annihilation photons generated when emitted positrons are absorbed in tissue [Raichle, 79; Webb, 88]. There are three main methods for measuring rCBF with positron emission tomography based on the Kety model; the steady state technique [Subramanyam, 77; Frackowiak, 80], the autoradiographic technique [Herscovitch et al, 83; Raichle et al, 83] and the dynamic technique [Alpert et al, 84; Huang et al, 82; Lammertsma et al, 89].

The steady state technique was the first developed. In this application, the patient inhales a ^{15}O labelled gas until the saturation concentration of the tracer in cerebral tissue has been achieved, at which time, a single PET scan is acquired. Since the tissue concentration is measured at saturation, the PET scan can be acquired over a long period of time, thus reducing the statistical noise in the image. However, this technique is time consuming and does not efficiently utilize the radiation dose administered to the patient [Lammertsma et al, 89].

The autoradiographic technique is considerably quicker than the steady state application. This technique requires a bolus injection of a tracer, usually $H_2{}^{15}O$, followed by a single PET scan shortly after injection. The entire procedure can take less than 5 minutes to complete [Kanno et al, 84].

The dynamic technique utilizes serial PET scanning with either the steady state or autoradiographic methods. As with the XeCT technique, dynamic scanning allows one to characterize the tracer tissue washin/washout curve so that both rCBF and the partition coefficient can be determined, simultaneously.

MRI generates three dimensional images of the interaction of nuclei with their surroundings in the presence of magnetic fields [Taylor et al, 88; Webb, 88]. Like the other tomographic imaging modalities, MRI can also be used in the application of the Kety model. However, techniques for measuring blood flow, which utilize MRI are still in the developmental stage. The substances currently being investigated as possible tracers are the contrast agent Gd-DTPA, which shortens T_1 and T_2 relaxation rates [Majumdar, 89], and the tracer agents D2O and ^{19}F, both of which provide MR signals at different Lamor frequencies than ^{1}H [Kim, 88; Eleff, 88]. Further work is required on these techniques before they can be clinically implemented.

1.3 Organization of Thesis

As mentioned in the introduction, one of the aims of this thesis is to compare the XeCT technique to a PET based rCBF measuring technique. The PET technique chosen for this comparison was the $C^{15}O_2$ buildup/dynamic PET technique. The Kety model, the XeCT and the $C^{12}O_2$PET techniques are described in chapter 2. The precision of rCBF measurements carried out using these two techniques is compared in chapter 3. The second goal of this thesis was to analyze a proposed simplification to the clinical application of the XeCT technique. This analysis is presented in chapter 4. Finally, chapter 5 is a general summary of the thesis.

Chapter 2

The Kety Model:

Xenon Enhanced Computed Tomography and

$C^{15}O_2$ Buildup Using Dynamic Positron Emission Tomography

Applications

2.1 Introduction

The aim of this chapter is to give a detailed outline of two techniques for measuring regional cerebral blood flow (rCBF); xenon enhanced computed tomography (XeCT) [Kelcz et al, 78; Drayer et al, 80] and $C^{15}O_2$ buildup technique using dynamic PET ($C^{15}O_2$) [Lammertsma et al, 89].

2.2 The Kety Model

In 1870, Fick derived a law, referred to as the Fick principle, to describe the uptake of a tracer substance in tissue [Kety 51]. The Fick principle is a special case of a more general postulate: the principle of mass conservation. This principle states that the amount of a substance carried into a tissue region (Q_a) in time Δt must be equal to the quantity disposed of by accumulation (Q_i) or conversion (Q_m) plus the amount exiting the region (Q_e):

$$\frac{Q_a}{\Delta t} = \frac{Q_i}{\Delta t} + \frac{Q_m}{\Delta t} + \frac{Q_e}{\Delta t} \qquad (1)$$

Let C_a represent the concentration of the tracer in arterial blood and C_v the concentration in venous blood. If it is assumed that the arterial blood and the venous blood provide the only significant pathways into and out of a tissue volume and if the rate of flow (F) of the two are equal, then $Q_a/\Delta t$ and $Q_e/\Delta t$ are given by FC_a and FC_v respectively. If it is also assumed that the tracer used is not metabolized, then Q_m equals zero and equation (1) can be rewritten as:

$$\frac{dQ_i}{dt} = F(C_a - C_v) \tag{2}$$

where Q_i is the amount of the tracer in the tissue. Equation (2) is referred to as the Fick principle.

If the volume of the tissue region is V_i, then:

$$\frac{dC_i}{dt} = \frac{dQ_i}{V_i dt} = \frac{F(C_a - C_v)}{V_i} \tag{3}$$

where C_i represents the concentration of tracer in tissue.

If the tissue is homogeneous with respect to the rate of perfusion and solubility of the tracer, then the following relation holds true at diffusion equilibrium [Kety 51]:

$$C_i = \lambda_i C_v \tag{4}$$

where λ_i is the tracer partition coefficient between tissue and blood. A partition coefficient is defined as the equilibrium ratio between the concentration of tracer in a certain tissue and its concentration in blood. The partition coefficient is usually expressed in units of g/ml or ml/ml. Equation (3) becomes:

$$\frac{dC_i}{dt} = f_i(C_a - \lambda_i C_i) \tag{5}$$

where f_i is defined as F/V_i and is the blood flow through a volume of tissue (ml/ml/min). A single value of f_i should describe the blood flow through the tissue compartment, V_i, provided the tissue volume and capillary volume in the compartment are well mixed.

In order to utilize relationship (4), the tracer diffusion equilibrium between blood and tissue must be instantaneous. Tracers that satisfy this criterion are referred to as freely diffusible [Kety, 51]. A more general statement of the Fick principle should include a diffusion factor, m_i, which ranges between 0 and 1, and represents the fraction of diffusion equilibrium achieved [Kety, 51]:

$$\frac{dC_i}{dt} = m_i f_i (C_a - C_v) \qquad (6)$$

The general solution to equation (6), assuming the arterial concentration to be a function of time is:

$$C_i(T) = C_i(T_o)\, e^{-k_i T} + k_i \lambda_i e^{-k_i T} \int_{T_o}^{T} C_a(t)\, e^{k_i t} dt \qquad (7)$$

where $C_i(T_o)$ is the concentration of the tracer in tissue at time zero and k_i is defined as the rate constant. k_i is related to f_i and λ_i by:

$$f_i = \frac{k_i \lambda_i}{m_i} \qquad (8)$$

If the concentration at T_o is zero then equation (7) reduces to:

$$C_i(T) = k_i \lambda_i e^{-k_i T} \int_{0}^{T} C_a(t)\, e^{k_i t} dt \qquad (9)$$

Equation (9) is commonly referred to as the Kety equation and serves as the basic foundation for the measurement of rCBF. For a freely diffusible tracer ($m_i = 1$), rCBF (f_i) can be calculated by determining the time rate of change of the

arterial concentration, $C_a(t)$, the specific tissue concentration at a time T, $C_i(T)$, and the local partition coefficient, λ_i.

Values of the partition coefficient for cerebral tissues have been determined for different tracers [Kety, 51; Herscovitch et al, 85; Veall et al, 65]. However, if the partition coefficient for a specific region of interest is incorrectly estimated, errors in the calculated blood flow can arise. For instance, if the region of interest contains abnormal tissue such as a carcinoma then it may prove difficult to accurately assign the correct partition coefficient. This problem can be eliminated by experimentally measuring the partition coefficient for each individual application of the Kety model.

The simplest method for determining the partition coefficient is to measure the equilibrium concentration of tracer in arterial blood and cerebral tissue. The partition coefficient is defined as the ratio of the two equilibrium concentrations:

$$\lambda_i = \frac{C_i(at\ equilibrium)}{C_a(at\ equilibrium)} \qquad (10)$$

However, this method is not very practical because it requires that tracer equilibrium in tissue be reached. Depending on the type of tissue under investigation and the tracer being used, equilibrium may take as long as 30 - 60 minutes to reach [Drayer et al 79].

It is possible to determine rCBF and λ_i simultaneously by monitoring the buildup of the tracer in cerebral tissue [Meyer et al, 81; Gur et al, 82; Lammertsma et al, 89]. In this method, the tissue concentration is sampled at various times as

it rises to its equilibrium level. The Kety equation is then fit to the experimentally measured tissue and arterial buildup curves to generate best fit estimates of the two parameters, k_i and λ_i. Blood flow is then calculated using equation (8). Both techniques discussed in the following sections use this curve fitting procedure to calculate values of rCBF.

2.3 Applications of the Kety Model

The rCBF measuring techniques: xenon-enhanced computed tomography (proposed in 1978 [Kelcz et al, 78]) and $C^{15}O_2$PET buildup using dynamic PET (proposed in 1989 [Lammertsma et al, 89]) are summarized in this section.

2.3.1 Tracer

The Kety model requires a tracer capable of crossing the blood-brain barrier. The stable gas xenon is used as the tracer in the XeCT technique and radioactive water ($H_2{}^{15}O$) is used in the $C^{15}O_2$PET technique. Both tracers readily cross the blood brain barrier.

With either technique, the patient inhales the tracer continuously throughout the duration of the study. For the XeCT technique, xenon is inhaled in the form of a xenon/oxygen mixture, typically 30 to 35 percent xenon, for a duration of about six minutes [Meyer et al, 81]. The inhaled xenon is absorbed by the blood in the lung capillary bed and is transported through the body via the arterial network. Upon reaching the brain, the xenon gas will cross the blood

brain barrier and buildup to a saturation concentration in the tissue. For the $C^{15}O_2$PET technique, radioactive water is administered by inhalation of $C^{15}O_2$. Water in blood is labeled via the ^{15}O transfer between carbon dioxide and water in the lung capillary bed [Subramanyam et al, 78]:

$$C^{15}O_2 + H_2O \rightarrow H_2C^{15}O_2 \rightarrow H_2^{15}O + CO_2 \qquad (11)$$

In this application, the patient inhales a mixture of $C^{15}O_2$ and air, at a concentration of 20 μC_i/ml, delivered at a rate of 500 ml/min [Lammertsma et al, 89]. As in the case of xenon, $H_2{}^{15}O$ will buildup to saturation in cerebral tissue.

2.3.2 Concentration of Tracer in Cerebral Tissue

The curve representing the buildup of tracer in cerebral tissue during inhalation is characterized by dynamic scanning. For XeCT, one or two baseline scans (scans prior to xenon inhalation) and four to six enhanced scans (scans during inhalation) separated by a time interval of about one minute are acquired [Meyer et al, 81; Good et al, 87a]. Because of xenon's high atomic number (Z = 54) and resulting k edge (34.6 keV), the combination of xenon and tissue will exhibit a greater attenuation of x-rays than tissue alone [Foley et al, 78]. As a result, the CT number of the tissue will increase with increasing xenon concentration. The increase in CT number, $\Delta HU(t)$, from the baseline scans to an enhanced scan can be directly related to the buildup of xenon in the tissue [Lee et al, 90a]:

$$\Delta HU(t) = CT_{enhanced} - CT_{baseline} = \alpha C_i(t) \qquad (12)$$

where α is a calibration factor, $CT_{baseline}$ is the CT number for a particular region of interest in a baseline scan and $CT_{enhanced}$ in the CT number for the same region of interest in an enhanced scan.

By plotting ΔHU(t) for each enhanced scan versus time, a curve is generated which represents the buildup of xenon in cerebral tissue. Figure 1 shows two such curves, one for gray matter and one for white [Bews et al, 90]. The data points on the curves represent theoretical values of ΔHU(t) obtained from each enhanced scan.

For $C^{15}O_2$PET, the tissue sampling protocol consists of 19 consecutive PET scans of the following length and order: 6 scans of 10 second duration, 9 scans of 20 second duration, 6 scans of 30 second duration and finally 3 scans of 60 second duration [Lammertsma et al, 89]. The activity measured in a scan can be directly related to the cerebral tissue concentration of $H_2{}^{15}O$ provided the sensitivity of the PET scanner is known. Figure 2 shows the theoretical buildup curves for grey and white matter for the initial six minutes of inhalation. Each point on the curves represents the total activity measured for a particular scan and the time of each point represents the beginning of a scan.

Unlike a CT scan, which can be considered instantaneous (a CT scan is typically acquired in two seconds), a PET scan represents activity measured over a longer time period. As a result, the Kety equation must be integrated over the scan time when applied to the $C^{15}O_2$PET technique:

$$Act(t) = \alpha \int_{t_1}^{t_2} C_i(t)\,dt = \lambda_i k_i \int_{t_1}^{t_2} \int_{0}^{t} C_a(u)\, e^{(-k_d(t-u))}\,du\,dt \qquad (13)$$

where Act(t) represents the activity measured during a scan, α is the sensitivity factor for the PET scanner, $(t_2 - t_1)$ is the time length of the scan, and k_d is the sum of the rate constant k, and the physical decay constant of ^{15}O (0.34 min^{-1}).

Figure 1

The enhancement in CT number for grey and white matter during the inhalation of a 33% xenon in oxygen mixture. The filled circles represent the sampling points during a typical clinical study.

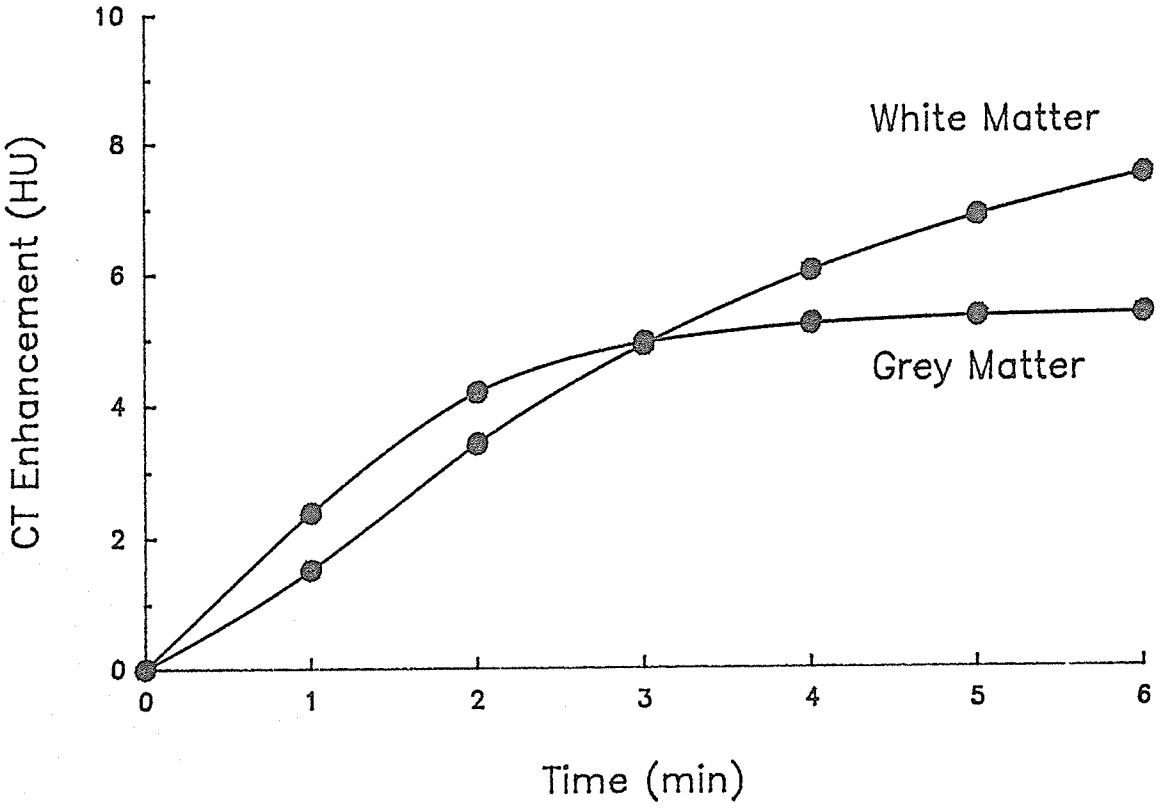
CT Enhancement (HU)
10
8
6
4
2
0
0
1
2
3
4
5
6
Time (min)
White Matter
Grey Matter

Figure 2

The activity measured in grey and white matter by a PET scanner during the inhalation of $C^{15}O_2$. The filled circles represent the sampling points during a typical clinical trial. Each point represents the total measured activity during the scan. The time of each point represents the beginning of a scan.

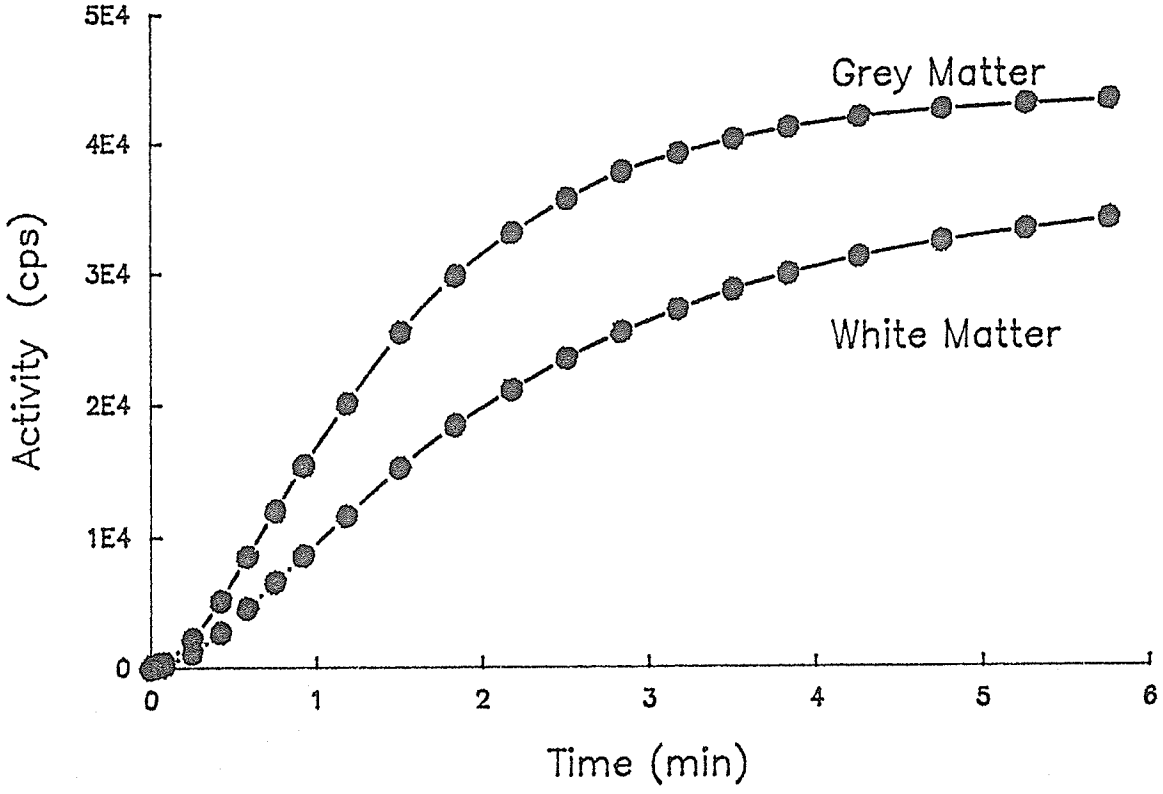
5E4
4E4
3E4
2E4
1E4
0
Activity (cps)
Grey Matter
White Matter
0
1
2
3
4
5
6
Time (min)

2.3.3 Concentration of Tracer in Arterial Blood

The arterial concentration of the tracer, $C_a(t)$, must also be measured as a function of time during the application of either technique.

For XeCT, $C_a(t)$ is usually determined indirectly by measuring the end-tidal xenon concentration in exhaled air, thus making the entire XeCT procedure non-invasive. The end-tidal portion of the expired air refers to air exiting the alveolar sacs of the lungs and it had been shown that the concentration of xenon in the end-tidal air is directly proportional to its concentration in the arterial blood [Obrist et al, 67]. The xenon concentration in expired air can be monitored using either a mass spectrometer or a thermoconductivity analyzer [Gur et al, 84], the latter being much less expensive and therefore more commonly used. The thermoconductivity of end-tidal air is linear with respect to the xenon concentration over the range of interest. Since the enhancement in CT number with respect to the buildup of xenon is tissue is also linear, the end-tidal xenon curve can be calibrated in terms of ΔHU [Meyer et al, 81].

To simplify the data analysis for the XeCT technique, $C_a(t)$ is assumed to be an exponential function of time [Good et al, 87a]:

$$C_a(t) = \beta C_{max}(1 - e^{-bt}) \qquad (14)$$

where C_{max} is the concentration of xenon in the inhaled gas mixture, b is a rate constant describing the rate at which the saturation concentration is reached and ß is a calibration constant, which relates expired air concentration to the arterial concentration. Figure 3 shows the buildup of xenon in end tidal air; the sampling

points represent measured end-tidal xenon concentration values from a patient study and the curve represents the best fit with equation (14) [Bews et al, 90]. Using this simplification, the Kety equation reduces to:

$$\Delta HU(t) = \alpha\beta\lambda_i k_i \left[1 + \frac{be^{-k_i t} - k_i e^{-bt}}{k_i - b} \right] \qquad (15)$$

The procedure for determining rCBF now consists of fitting equation (14) to the end-tidal data to derive b, and then fitting the Kety equation, equation (15), to the cerebral tissue data to determine rCBF. By characterizing the end-tidal xenon concentration data with equation (14), the need for numerical integration in the fitting procedure is eliminated, thus reducing the computational time.

For $C^{15}O_2$PET, $C_a(t)$ is measured directly [Lammertsma et al, 89]. Arterial blood is drawn continuously throughout the study via a catheter inserted in the radial artery. The blood passes through a tube which is looped around a cylindrical scintillator sensitive to beta radiation. Figure 4 shows a side view of the beta detector unit [Weinberg et al, 88]. The scintillator response is recorded by a single channel analyzer whose output, in turn, is fed to a scaler module, the content of which is recorded every two seconds. The recorded arterial blood activity is cross-calibrated to the PET scanner. Figure 5 shows the measured activity in arterial blood as a function of time during a typical patient study [Lammertsma et al, 89].

Figure 3

Patient breathing curve during continuous inhalation of a 33% xenon in oxygen mixture. The filled circles represent experimentally measured values of the end-tidal xenon concentration in expired air. The solid line is the best fit of a single exponential to these data.

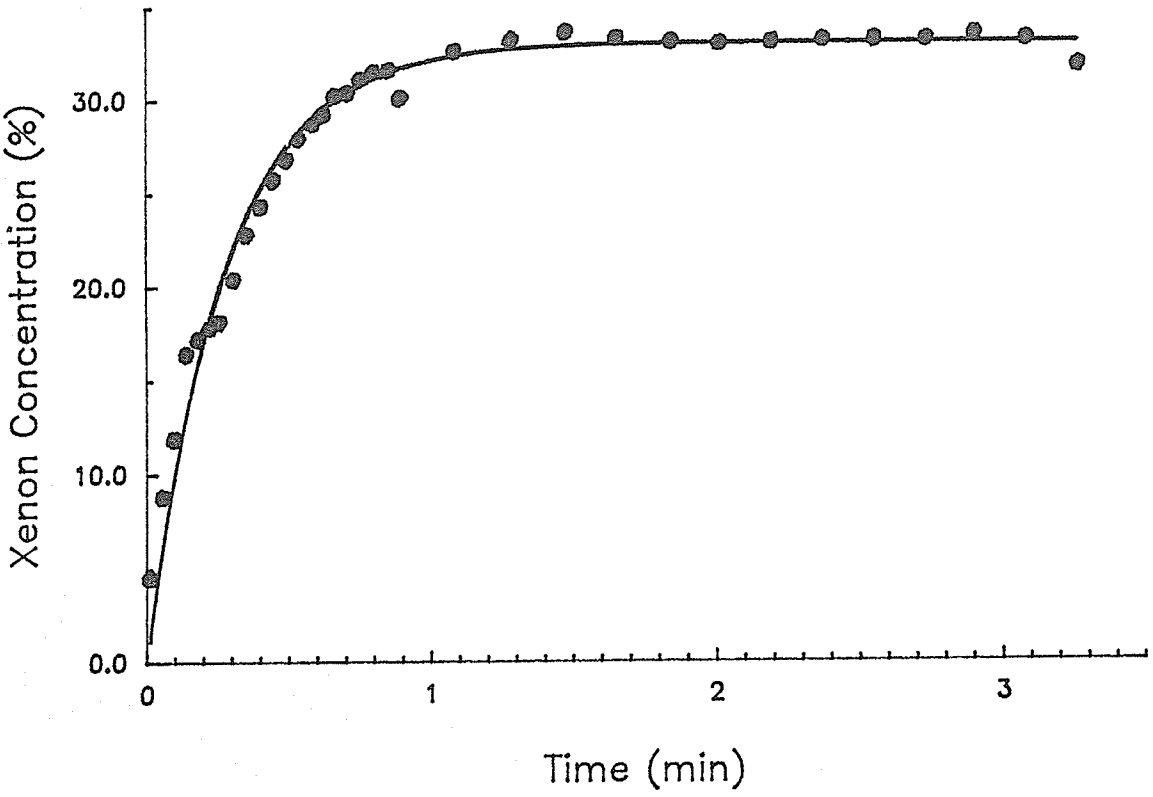
Xenon Concentration (%)
30.0
20.0
10.0
0.0
0
1
2
3
Time (min)

Figure 4

Side View of the beta detector unit used in the $C^{15}O_2$PET technique to measure the activity of $H_2{}^{15}O$ in arterial blood [Weinberg et al 88].

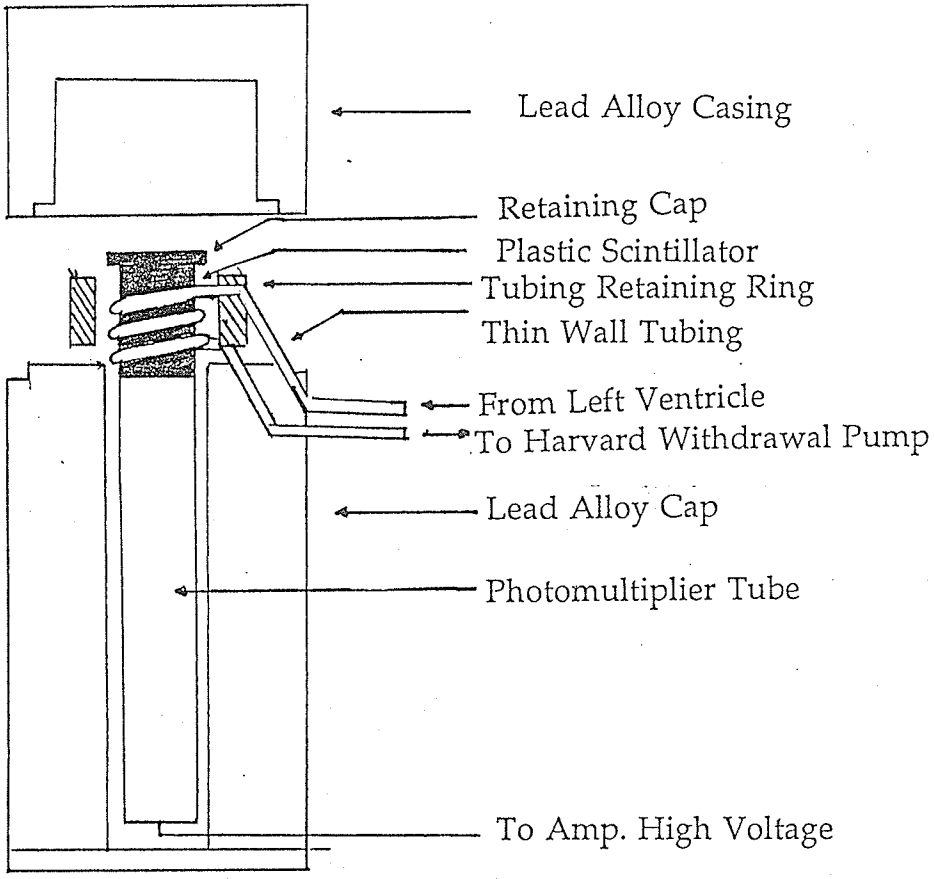
Lead Alloy Casing
Retaining Cap
Plastic Scintillator
Tubing Retaining Ring
Thin Wall Tubing
From Left Ventricle
To Harvard Withdrawal Pump
Lead Alloy Cap
Photomultiplier Tube
To Amp. High Voltage

Figure 5

Measured arterial activity curve during continuous inhalation of $C^{15}O_2$. The sampling points represent the activity measured by the beta counter every two seconds [Lammertsma et al, 89].

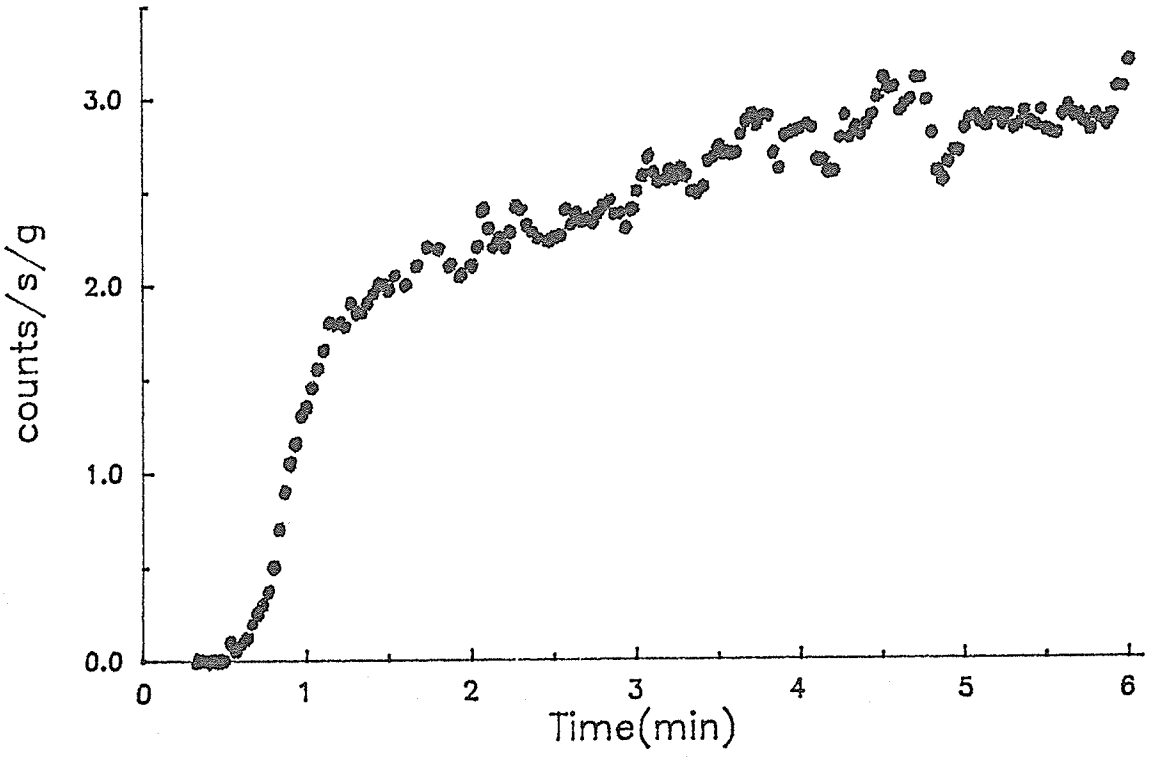
counts/s/g
3.0
2.0
1.0
0.0
0
1
2
3
4
5
6
Time(min)

2.4 Potential Sources of Error with the two Applications

The objective of this section is to outline potential sources of error in the XeCT and $C^{15}O_2$PET techniques. As with the previous section, both techniques will be discussed simultaneously to emphasize similarities and differences.

2.4.1 Potential Sources of Error Associated with the Tracer

The Kety model is a single compartment model; that is, a single value of flow should adequately describe the passage of the tracer through the tissue volume. There has been no evidence to dispute the adequacy of this model for describing the perfusion of xenon. However, there has been concern that the Kety model is not suitable for describing the tissue perfusion of $H_2{}^{15}O$. It has been discovered from blood flow measurements using other PET techniques with $H_2{}^{15}O$, that results are often dependent on the time length of the study [Gambhir et al, 87]. It has been suggested that this time dependence is a result of the water movement through tissue consisting of two components: a fast component representing freely exchangeable water and a slow component representing water that is bound to various molecular compounds in tissue [Gambhir et al, 87]. Under these circumstances, a two compartmental model would be expected to better describe the water movement. The $C^{15}O_2$ buildup technique has produced blood flow measurements which appear to be independent of the study duration [Lammertsma et al, 89]. This independence suggests that the time dependence observed with other techniques may be due to other sources of error such as the

time delay between the cerebral and arterial activity data or the dispersion of the arterial function [Lammertsma et al, 89]. These errors are described in section 2.4.3.

Another restriction of the Kety model is that the tracer used must be freely diffusible. This restriction means that the diffusion of the tracer through the tissue must be rapid enough that its movement is only dependent on blood flow. If this criterion is not satisfied, blood flow measurements will depend on the diffusion rate of the tracer. Although xenon is considered freely diffusible, water is not [Eichling et al, 74]. In fact, it has been shown in animal studies, that the blood flow measured using labelled water will be progressively underestimated as flow increases, due to the restricted diffusion of water [Raichle et al, 83]. Fortunately, in humans this underestimation is small for normal flow rates [Lammertsma et al, 81]. However, this limitation should be duly noted when flow rates are high.

An underlining assumption for the successful application of either XeCT or $C^{15}O_2$PET is that the tracer used will not effect blood flow. With $H_2{}^{15}O$, this is a reasonable assumption since water is found naturally in cerebral tissue. On the other hand, xenon is not found naturally in the body, and is known to have side effects if inhaled at relativity high concentrations (greater that 30 percent) for prolonged periods of time (greater than 4 minutes) [Gur et al, 85].

Xenon is an anesthetic [Meyer et al, 81] and at high concentrations, it can affect blood flow [Junck et al, 85; Gur et al, 85]. The obvious solutions to this

problem would be to reduce the concentration inhaled and/or limit the inhalation time. However, limiting the inhalation time to less than 4 minutes makes it is impossible to reach the tissue saturation in some tissues, notably white matter. Regardless of whether the partition coefficient is measured using the ratio of the equilibrium concentrations of xenon in blood and tissue (equation 10) or curve fitting, its accuracy and precision will depend on being able to sample tissue concentration at saturation. Although attempts have been made to extrapolate to the saturation value [Drayer et al, 79], the calculated partition coefficient for white matter is often erroneous [Meyer et al, 81; Bews et al, 90].

Reducing the percent xenon inhaled will adversely effect the accuracy of rCBF measurements by reducing the signal to noise ratio (SNR) in the serial scans used to characterize the buildup of xenon in tissue (the dependence of the rCBF measurements on SNR is discussed in the next section). In an effort to balance the effects of xenon on rCBF and the accuracy of the XeCT technique, the concentration of xenon used in clinical studies is typically around 35% and the study duration about 4 to 6 minutes [Yonas et al, 85].

2.4.2 Potential Sources of Error Associated with Measuring the Concentration of Tracer in Cerebral Tissue

Both XeCT and $C^{15}O_2$PET use serial scanning to characterize the tissue buildup curve. In order for this characterization to be successful, the measurement of the tracer concentration in tissue from the individual scans

should be as precise and accurate as possible. The precision and accuracy of these measurements will be limited by the noise in the images. In fact, noise is one of the dominant sources of error in both techniques [Rottenberg et al, 82; Good et al, 87b; Lammertsma et al, 89] and is the topic of the next chapter. For both CT and PET, noise is primarily due to the statistical nature of the detection of transmitted/emitted photons. Scattered photons can also contribute to the noise.

There are three basic methods for reducing the effect of image noise. Firstly, the SNR in the images can be improved by increasing the concentration of the tracer administered. Unfortunately, for XeCT, the concentration of xenon inhaled should remain below 35% for the reasons mentioned previously. With $C^{15}O_2$PET, the concentration of $C^{15}O_2$ inhaled can be increased, but only at the expense of increasing the radiation dose delivered to the patient.

A second possible method of reducing the effects of noise is to acquire more scans during the study. For XeCT, multiple baseline scans can be collected and averaged to reduce the magnitude of the noise [Good et al, 87b]. Increasing the number of enhanced scans will improve the sampling of the tissue buildup curve. However, in both cases, the patient radiation dose is increased. For $C^{15}O_2$PET, the radiation dose is entirely independent of the number of scans obtained. The only restriction on sampling the buildup curve is insuring that a sufficient number of events are recorded in each individual scan. As such, a relatively large number of scans can be acquired to better characterize the buildup

curve. This is why nineteen consecutive scans are obtained for the $C^{15}O_2$PET technique, compared to only six scans for XeCT.

The final method for reducing the effect of noise is to use regions of interest (ROI) to calculate the average signal enhancement rather than individual pixels [Drayer et al, 79; Bews et al, 90; Lammertsma et al, 89]. By using ROIs, the standard deviation of the noise can be reduced through pixel averaging. It has been suggested that for XeCT, ROIs should be greater than 40 mm^3 in order to obtain sufficient precision in CT numbers [Drayer, 79]. For $C^{15}O_2$PET, the smallest ROI reported in the literature was 4 cm^3 [Lammertsma et al, 89]. Quite clearly, there is a trade off between ROI size and resolution.

Although the use of ROIs for calculating rCBF reduces the effect of noise, the effect of another potential source of error, tissue inhomogeneity, will increase. Recall that the Kety equation is a single compartment model, which means that for a given volume of tissue, a single value for blood flow and partition coefficient will be generated. However, cerebral tissue is comprised of two main types of tissue (grey matter and white matter) and often the ROI will contain a mixture of both. It has been shown that for a inhomogeneous tissue volume, the Kety equation will produce biased estimates of the average values of rCBF and λ_i [Good et al, 87b; Kanno et al, 85; Koeppe et al, 84; Herscovitch et al, 83]. With XeCT, this bias will lead to an underestimation of blood flow of the order of ten percent for a tissue volume containing approximately equal amounts of grey and white matter [Good et al, 87b]. Similar results have been reported from blood

flow studies using various PET techniques [Kanno, 84; Koeppe, 85; Herscovitch, 83]. Although, the reported severity of this bias varies from one study to another, estimated errors have ranged from -3.7% [Herscovitch et al, 83] to -20% [Koeppe et al, 85]. The effect of tissue inhomogeneity was not discussed in the article on the $C^{15}O_2$ buildup technique [Lammertsma et al, 89]. However, judging by previous reports and the large regions of interest used in the $C^{15}O_2$ buildup article, tissue inhomogeneity must certainly have some detrimental effect of the accuracy of this technique.

Errors introduced in rCBF measurements by noise is considerably larger that the error introduced by tissue inhomogeneity [Good et al, 87b; Lammertsma et al, 89]. As such, regions of interest must be used and the effect of tissue inhomogeneity endured.

Two factors, unique to PET, which can also reduce the precision and accuracy of rCBF measurements, are random coincidences (coincidence events due to two photons generated through separate annihilation events [Ter-Pogossian, 81]) and deadtime (the time period following detection of a photon for which a detector will not accept any more events [Derenzo et al, 75]). Fortunately, because of the low count rates used in the $C^{15}O_2$PET technique, the effect of these two factors should not be significant [Lammertsma et al, 89].

Another potential source of error in characterizing the tissue buildup is ensuring the serial scans are aligned so that the same ROI is obtained in each scan. This alignment requires that the patient remain motionless throughout the

entire study, a condition that can be very difficult to satisfy. As a result, misregistration of images is a frequent problem. Movements that occur in directions within the plane of the image can be removed with postprocessing (pixel shifting) while movements in the axial direction are very difficult to correct [Gur et al, 82]. To reduce the effect of motion, a head holder which fits snugly around the patient's head, securing it firmly in position, should be used [Gur et al 82].

In both XeCT and $C^{15}O_2$PET, inaccuracies in the measured calibration factors can lead to errors in the rCBF estimates. For XeCT, the calibration factor relating the enhancement in CT number to the concentration of xenon in brain tissue must be known. This factor can be determined for a specific scanner by measuring the CT number for various known concentrations of xenon in a brain phantom [Lee et al, 90a]. It is important that this calibration factor remain constant throughout a patient study, and be independent of spatial position in the scan. However CT drift (the systematic change in CT number with time) [Kearfott et al, 83] and beam hardening (the increase in mean energy of the x-ray beam as it passes through tissue) [Lee et al, 90a] can jeopardize the constancy of this calibration factor. For the $C^{15}O_2$PET technique, a calibration factor relating the activity measured in the arterial blood counting apparatus to the activity measured in the PET scanner must be known. This calibration factor is determined by counting the same radioactive blood samples in each apparatus. Any uncertainty in the count rates recorded by the two apparatus could introduce

error into the value of this calibration factor. Fortunately, both XeCT and $C^{15}O_2$PET are relatively insensitive to errors in their respective calibration factors [Lee et al, 90a; Lammertsma et al, 89].

2.4.3 Potential Sources of Error Associated with Measuring the Concentration of Tracer in Arterial Blood

Both the XeCT and the $C^{15}O_2$PET techniques require that the arterial buildup curve, $C_a(t)$, be determined simultaneously with the tissue buildup curve, C(t). A potential source of error with the measurement of $C_a(t)$ is the time difference between the arrival of the tracer in cerebral tissue and its arrival to the arterial sampling location (ie. the lungs for XeCT and a radial artery for $C^{15}O_2$PET. If not accounted for, this time delay can introduce a large error in the rCBF estimates [Dhawan et al, 86; Good et al, 87a]. For instance, with XeCT it has been estimated that a time delay of 6 seconds, which is typical in clinical studies, can produce a 14% error in calculated flow values [Good et al, 87a].

The time delay can be incorporated into the Kety model by treating it as a third independent variable in the curve fitting procedure [Fatouros et al, 87; Lammertsma et al, 89]. As well, for XeCT, it can be estimated by extrapolating the tissue buildup curve to the time axis, assuming the enhancement in CT number rises smoothly [Fatouros et al, 87].

A potential source of error unique to the $C^{15}O_2$PET technique is the dispersion of the arterial function as it passes through the radial artery and the

blood counting apparatus [Iida et al 86]. With XeCT, dispersion is not a significant problem because $C_a(t)$ is measured from the expired air and therefore the dipersion of the function as it passes through the arterial network is of no concern. Like the time delay, the dispersion of the arterial function can be corrected for by incorporating it into the fitting procedure [Lammertsma et al, 89]. However, due to counting statistics, these phenomena can only be incorporated when very large regions of interest (whole brain) are used. For smaller regions, values determined from large regions must be used.

For XeCT, errors can arise as a result of approximating the arterial data with a single exponential function instead of using the measured arterial data directly. It has been estimated that errors in flow values of the order of 5% can be introduced [Good et al, 87a]. This potential error can be reduced by fitting the arterial data with a more flexible function such as a single exponential with a linear term [Good et al, 87a] or a double exponential [Fatouros et al, 87]. Unfortunately, the computation time associated with curve fitting will be increased.

Chapter 3

Measurement of regional Cerebral Blood Flow:

A Comparative Study of Two Techniques

3.1 Introduction

The two techniques for measuring rCBF outlined in chapter two were xenon enhanced computed tomography (XeCT) and $C^{15}O_2$ buildup using dynamic PET ($C^{15}O_2$PET). Both require that the temporal buildup of a tracer in cerebral tissue be determined. Using a curve fitting routine, the Kety equation is fit to the buildup data to generate estimates of the rate constant k and the partition coefficient λ. rCBF is the product of these two parameters. With either technique, the cerebral buildup is determined by a series of tomographic images obtained while the patient continuously inhales the tracer. Figures 1 and 2 show the theoretical buildup curves for grey and white matter for each technique. The data points represent the times at which the curves are typically sampled through scanning.

Noise is present in both CT and PET images and is primarily due to the statistical nature of the detection of transmitted/emitted photons by the respective scanners. This noise introduces an uncertainty in the measurement of the tracer concentration from the individual scans and thus leads to error in the fitted estimates of k, λ and rCBF. It has been stated that image noise is one of the dominant sources of error with either technique [Good et al, 87b; Lammertsma el al, 89]. The objective of this chapter was to compare XeCT and $C^{15}O_2$PET by analyzing the effect image noise has on the precision of the rCBF measurements obtained by both techniques. This comparison was carried out using Monte Carlo type computer simulations.

3.2 Method

3.2.1 Monte Carlo Simulations

The algorithm for the Monte Carlo simulation is as follows:

step 1) Using the Kety equation (equation 9) with typical values of k, λ, and arterial tracer concentration data, a theoretical curve describing the buildup of a specific tracer in cerebral tissue is generated.

step 2) A number of points is selected from the theoretical tissue buildup curve to represent the scans obtained during a typical clinical study.

step 3) A random number generator with zero mean and unit variance is used to simulate the noise present in the scans. The output from the generator is multiplied by a constant to provide noise of the desired variance and then added to the sampling points to yield a noisy data set.

step 4) The Kety equation is then refit to the noisy data to generate 'best fit' estimates of λ and k. rCBF is the product of k and λ.

The entire procedure is repeated 1000 times to yield distributions for λ, k and rCBF for a particular magnitude of image noise. Distributions are generated for a range of noise levels (described by different vaiances) and are used to quantify the effect of noise on the precision of blood flow measurements by noting the spread of the distribution generated.

3.2.2 XeCT Simulations

The Monte Carlo noise analysis for the XeCT technique has been previously performed [Bews et al, 90]. In this section an overview of that work will be presented.

The single integral Kety equation was used in this study because the duration of a typical CT scan is quite short (two seconds) and can therefore be ignored. The buildup of xenon in cerebral tissue was determined by the enhancement in CT number observed during serial scanning (equation 12).

With the XeCT technique, the arterial concentration of the tracer was determined indirectly by monitoring the end-tidal concentration of xenon in the patient's expired air (chapter 2.3.3). In order to reduce the computation time, the end-tidal concentration of xenon is approximated by a single exponential function (equation 14). C_{max}, the saturation concentration of xenon in expired air, was equal to 33%, the percent xenon in a Xe/O_2 mixture inhaled in a typical clinical trial. The value of the rate constant, b, was 2.5 min^{-1} and was determined by fitting the exponential function to typical clinical data (figure 3). The form of the Kety equation used in the simulations is equation (15).

Six sampling points separated by one minute intervals plus one baseline point (at t = 0) were used to represent a typical clinical scanning protocol.

The enhancement in CT number for each scan is determined by subtracting the baseline scan from the enhanced scan, as discussed in section 2.3.2. Since the determination of the tissue concentration of xenon relies on the subtraction of

images, noise was added to both the enhanced scans and the baseline scan.

In order to compare the XeCT and with the $C^{15}O_2$PET simulations, the XeCT results were converted from error in flow versus CT noise [Bews et al, 90] to error in flow versus region of interest (ROI) size, where a ROI is defined as a group of neighboring voxels and has units (dimension)^3. For this conversion, it was necessary to use the following scanner specifications: the standard deviation for a single pixel, σ, was 3.5 HU [Lee, 90b], the image matrix was 512 x 512, with each voxel having dimensions 0.5 mm x 0.5 mm x 10 mm. This standard deviation was obtained on a GE9800 CT scanner with the GE quality control water phantom and the following technique factors: 120 kVp, 170 mA, 2 second scan duration, 1 cm slice thickness, and a 512 x 512 matrix.

The standard error, SE, for a ROI in an image with uncorrelated noise is:

$$SE = \frac{\sigma}{(number\ of\ pixels \in ROI)^{1/2}} \qquad (16)$$

Let A_{ROI} be the area of the square ROI (cm^2) and d be the dimension of a pixel (cm). Equation (16) can be written as:

$$SE = \frac{\sigma\ d}{(A_{ROI})^{1/2}} \qquad (17)$$

Since d = 0.05 cm and σ = 3.5 HU:

$$A_{ROI} = \frac{2.5 \times 10^{-3}}{1.5}\left[\frac{3.5}{SE}\right]^2 \qquad (18)$$

Equation (18), was used to derive A_{ROI} for magnitudes of CT noise.

3.2.3 $C^{15}O_2$PET Simulations

The shortest duration of a PET scan used in the application of the $C^{15}O_2$PET technique was 10 seconds [Lammertsma et al, 89]. Since a PET scan does not measure the instantaneous concentration of a tracer, the Kety equation must be integrated over the duration of the scan (equation 13).

The single exponential function used in the XeCT study to represent $C_a(t)$ was chosen for the $C^{15}O_2$PET simulations so that the two procedures were as similar as possible. For the same reason, b was set equal to 2.5 min^{-1}. The value of C_{max} was chosen so that the total count rate measured at tracer saturation was approximately 44K true events/s/scan [Lammertsma et al, 89]. The form of the Kety equation used in the simulations was:

$$Act(t) = k\lambda C_{MAX}\left[\frac{(t_2 - t_1)}{k_d} + \frac{(e^{-bt_2} - e^{-bt_1})}{b(k_d - b)} + \frac{b(e^{-k_d t_2} - e^{-k_d t_1})}{k_d^2(b - k_d)}\right] \qquad (19)$$

where Act(t) is the activity measured in a PET scan during the time interval $t_2 - t_1$.

The time and duration of the sampling points taken from the tissue buildup curve were as follows [Lammertsma et al, 89]: six consecutive scans with duration of 10 seconds each, followed by nine consecutive scans of 20 seconds each, and finally four consecutive scans of 30 seconds each. The entire duration of the study was six minutes, identical to the duration of the XeCT study.

For error analysis it was necessary to choose a slice thickness and a pixel

size. A slice thickness of 1 cm was chosen so as to be comparible with that used in the XeCT study. A pixel size of 0.5 cm was chosen assuming a 30 cm field of view with a 64 x 64 matrix. The standard deviation of the noise, σ, associated with a pixel was calculated using the following formula [Budinger et al, 77]:

$$\frac{signal}{\sigma} = \frac{(total\ number\ of\ events/scan)^{1/2}}{1.2\ (number\ of\ pixels/scan)^{3/4}} \qquad (20)$$

where the signal is the mean number of counts in a pixel. The derivation of this formula is given in the appendix I. The standard error associated with a ROI is given by equation (17) where d is equal to 0.5 cm and σ is determined by equation (20).

Equation (20) describes the signal-to-noise ratio, SNR, for a cylindrical distribution of uniform activity. The values of SNR generated from this formula are very similar to those quoted for the ECAT III PET scanner [Hoffman et al, 83], which was the scanner used in the clinical trials of the $C^{15}O_2$PET technique [Lammertsma et al, 89].

The cylindrical distribution is considered a worst case senerio for evaluating the SNR [Hoffman et al, 83]. In a typical clinical scan, the SNR can often be improved by taking into account the contrast between the ROI and its background [Budinger et al, 78]. However, for images of the brain using a diffusible tracer, the contrast between the different tissue types is small (figure 2 illustrates the similarity between the saturation levels for grey and white matter for the diffusible tracer $H_2{}^{15}O$). Therefore, this formula should provide a

reasonable description of the SNR in the images used in this study.

3.3 Procedure

The most important factor determining the precision of flow values measured with either technique is the SNR in the acquired scans. The SNR expresses the level of uncertainty associated with the tracer concentration measurement in each scan and as such, the greater the SNR, the more precise the fitted flow values.

With either technique, the SNR can easily be improved by increasing the concentration of the tracer administered, and employing ROIs in the flow calculations; the negative effects of a low SNR meanwhile, can be reduced by optimizing the scanning protocol. A higher concentration of inhaled xenon will result in a greater enhancement in CT number [Bews et al, 90] and a higher inhaled concentration of $C^{15}O_2$ will result in greater tissue activity (SNR is proportional to the square root of the number of photons detected [Budinger et al, 77]). The SNR will be improved by using ROIs in the flow calculations because the noise can be reduced by pixel averaging. The scanning protocol is important because if the cerebral buildup curve is well sampled, the curve fitting procedure can offset the error introduced by the noise in the individual scans.

To determine the relationship between the precision of rCBF measurements and SNR, the XeCT and $C^{15}O_2$PET simulations were run for grey matter (rCBF = 0.8 ml/ml/min) and white matter (rCBF = 0.4 ml/ml/min) over a range of ROIs

(0.25, 0.5, 0.75. 1.0, 1,5, 2.0, 3.0 cm^3). One thousand simulations were run for each ROI size using the technical factors (ie. the scanning protocol, resolution, etc.) described in the previous section. For the XeCT simulations, input values of k = 1.0 min^{-1} and λ = 0.8 ml/ml for grey matter and k = 0.29 min^{-1} and λ = 1.4 ml/ml for white matter were used [Good et al, 87b]. For the $C^{15}O_2$PET simulations, the input values used were k = .8 min^{-1} and λ = 1.0 ml/ml for grey matter and k = 0.47 min^{-1} and λ = 0.86 ml/ml for white matter [Herscovitch et al, 84].

All $C^{15}O_2$PET simulations discussed so far, had a steady state count rate of 44K events/s/scan for grey matter, which corresponded to the patient continuously inhaling 20μCi/ml of $C^{15}O_2$ at a rate of 500 ml/min [Lammertsma et al, 89]. To demonstrate the effect of increasing the concentration of tracer administered, the $C^{15}O_2$ simulations were repeated, for grey matter and a ROI of 2.0 cm^3, with a count rate equal to 66K events/s. This higher count rate corresponds to an inhaled concentration of 30μCi/ml, assuming a linear relationship between the concentration of the $C_2{}^{15}O$ inhaled and the count rate recorded.

The disadvantage with using a higher concentration of $C^{15}O_2$ is an increased patient radiation dose. To determine if the improvement in precision obtainable with a higher tracer concentration can be maintained when the study duration is decreased (and hence, offset the increase in dose due to a higher concentration), the $C^{15}O_2$PET simulations were repeated with the study duration of four minutes and an inhaled concentration equal to 30μCi/ml. An inhaled

concentration of 30 μCi/ml with a study duration of 4 minutes will result in the same patient dose as a concentration of 20 μCi/ml with a duration equal to 6 minutes. The scanning protocol chosen for the four minute study was as follows: twelve consecutive scans with duration of ten seconds each, followed by four scans of fifteen seconds each and finally three scans of twenty seconds each. This protocol consists of the same number of scans as the six minute scanning protocol.

Although a higher concentration of xenon would improve the precision of rCBF measurements obtained with the XeCT technique [Bews et al, 90], it has been determined that the concentration should remain below 33% due to the side-effects of xenon (section 2.4.1.). Therefore, XeCT studies with a xenon concentration greater than 33% were deemed to have no clinical value and were not simulated.

Finally to study the dependence of the precision on the scanning protocol, XeCT simulations were run for grey matter and a ROI of 2 cm^2, using 19 scans (same number used in the $C^{15}O_2$ technique), each separated by 20 seconds. Likewise, $C^{15}O_2$ simulations were run for grey matter and a ROI of 2 cm^2 with only seven scans, separated each by one minute, starting at time zero. The duration of each scan was the same as the corresponding scan in the 19 scans protocol.

3.4 Results

Figures 6(a) and (b), represent rCBF distributions from the XeCT and $C^{15}O_2$PET simulations respectively for grey matter and a ROI equal to 2.0 cm^3. These distributions show the relative probability of obtaining a particular flow value when fitting the Kety equation to data collected with this ROI size. The larger the spread of these distributions, the worse the precision of a rCBF calculation. The spreads are quantified by the 5 and 95 percentiles (dashed lines), the values of flow for which five percent of the distribution lies below or above respectively. Percentiles are used to quantify the spread rather than standard deviations because of the non-normal shape of the distributions [Bews et al, 90].

The uncertainty in a grey matter flow measurement, for the two techniques is illustrated in figure 7(a) as a function of ROI. The dotted line represents the true input flow value (0.8 ml/ml/min). The solid lines represent the 5 and 95 percentiles from the $C^{15}O_2$PET simulations and the dashed lines represent the corresponding percentiles from the XeCT simulations. The uncertainty in a white matter flow measurement as a function of ROI is illustrated in figure 7(b). For white matter, the true input flow value was 0.4 ml/ml/min.

Table 1 lists the 5 and 95 percentiles from the $C^{15}O_2$PET simulations for grey matter, a ROI = 2.0 cm^3, and for three different scenarios: inhaled $C^{15}O_2$ at a concentration equal to 20μCi/ml and a study duration equal to 6 minutes; inhaled $C^{15}O_2$ at a concentration equal to 30 μCi/ml and a study duration equal to 6 minutes; and $C^{15}O_2$ at a concentration equal to 30μCi/ml and a study

duration equal to 4 minutes. Included in the table are the percentiles from the XeCT simulations for a 2.0 cm^3 ROI. The percent difference between the spreads of the various distributions are also given.

Table 2(a) shows the 5 and 95 percentiles, as well as the spread of the distributions (95% - 5%) for two different $C^{15}O_2$PET scanning protocols, 19 scans and 7 scans respectively. These results were obtained for grey matter and a ROI of 2 cm^3. The percent decrease in the spread of the distribution going from 7 to 19 scans is also given. The corresponding results for the XeCT simulations are given in table 2(b). In this case, 6 and 18 enhanced scans protocols were compared.

Figure 6

Grey matter flow distribution for a 2.0 cm^3 region of interest generated from (a) the XeCT simulations and (b) the $C^{15}O_2$PET simulations. The dashed lines represent the 5 and 95 percentiles of the distribution.

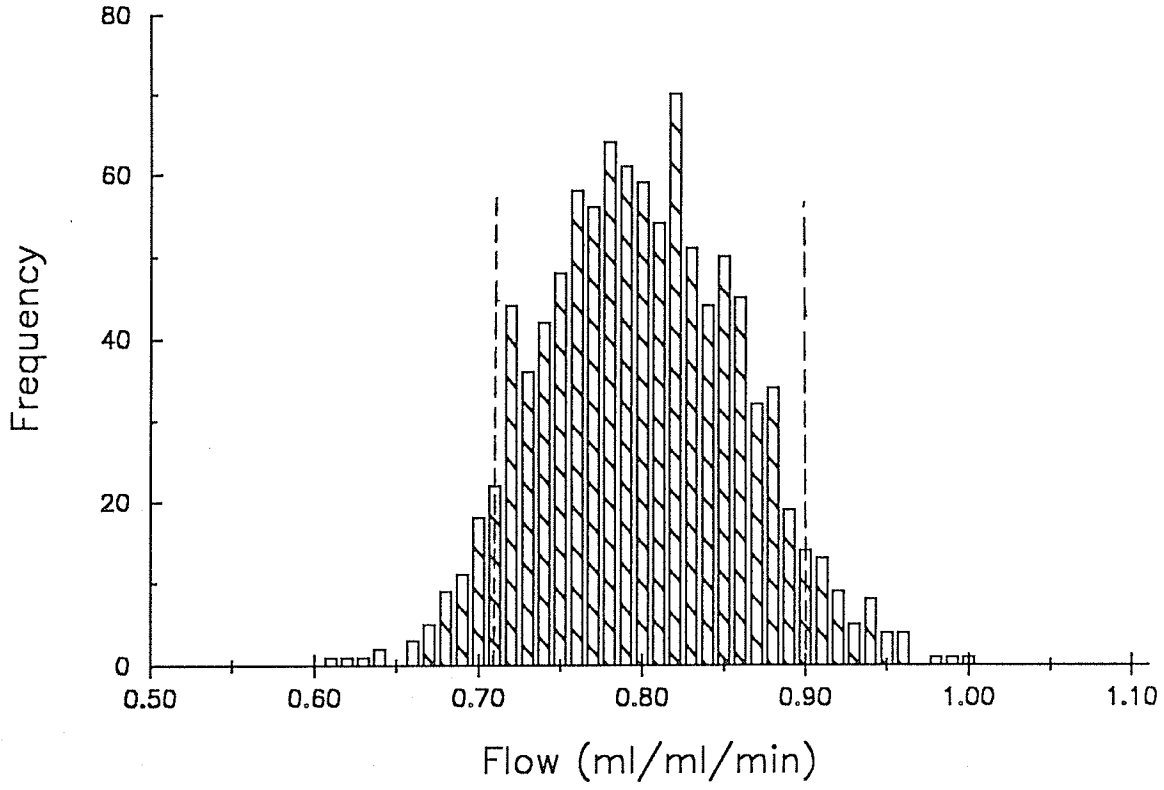
80
60
40
20
0
Frequency
0.50
0.60
0.70
0.80
0.90
1.00
1.10
Flow (ml/ml/min)

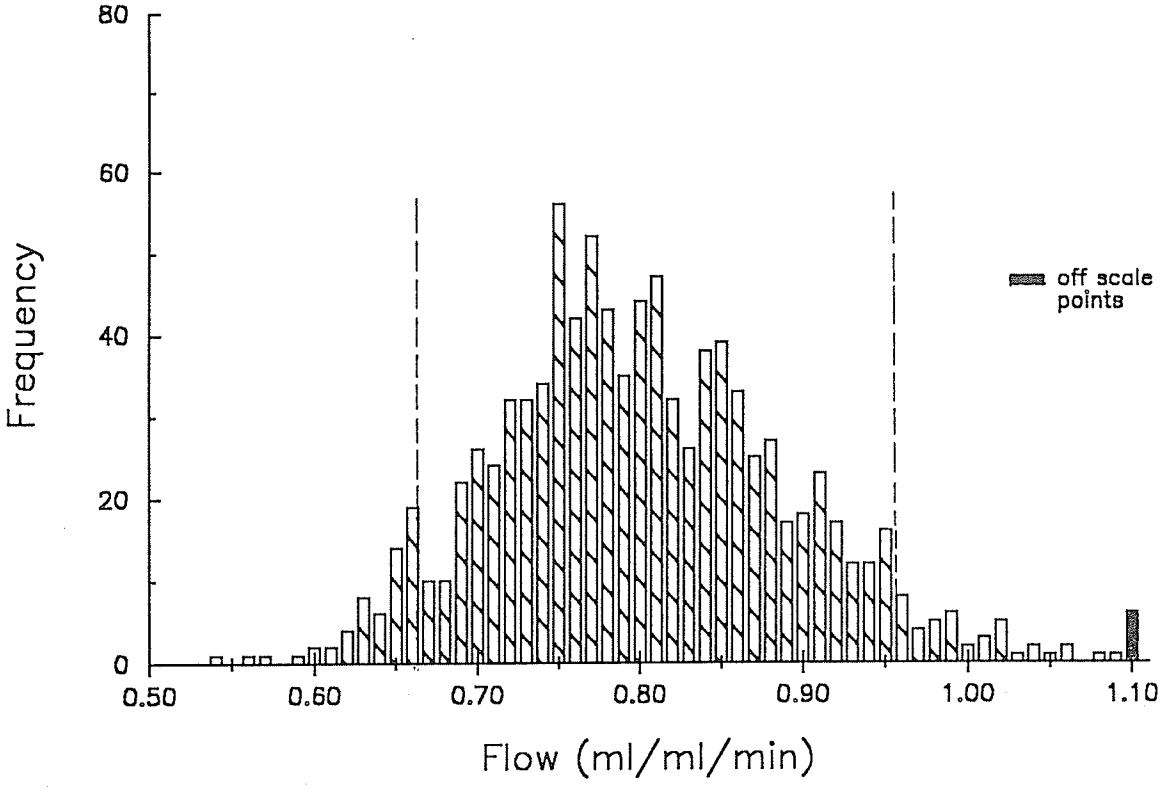
80
60
40
20
0
Frequency
0.50
0.60
0.70
0.80
0.90
1.00
1.10
Flow (ml/ml/min)
off scale points

Figure 7

(a) The error arising from noise in grey matter flow measurements as a function of ROI size for both the XeCT and the $C^{15}O_2$PET techniques. The dotted line represents the input flow value to the simulations. The solid line represents the 5 and 95 percentiles from the $C^{15}O_2$PET simulations and the dashed lines represent the corresponding percentiles from the XeCT simulations. (b) The error arising from noise in white matter flow measurements.

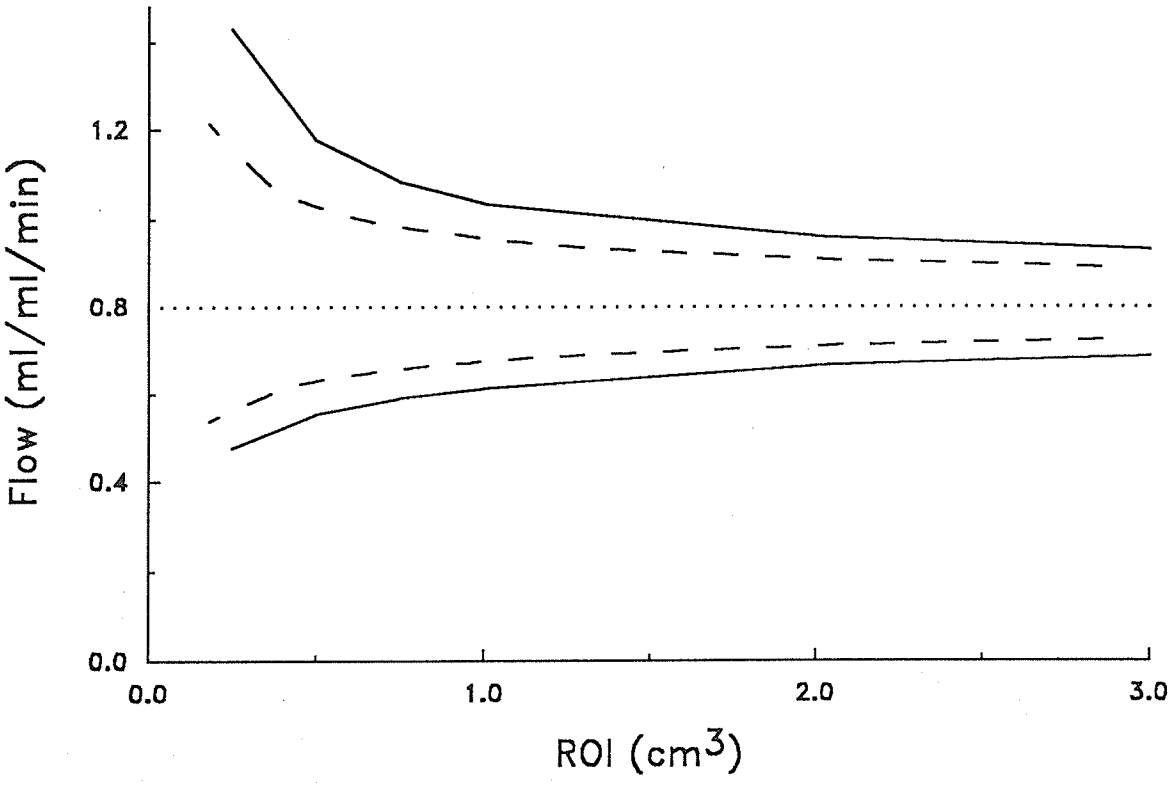
Flow (ml/ml/min)
1.2
0.8
0.4
0.0
0.0
1.0
2.0
3.0
ROI (cm3)

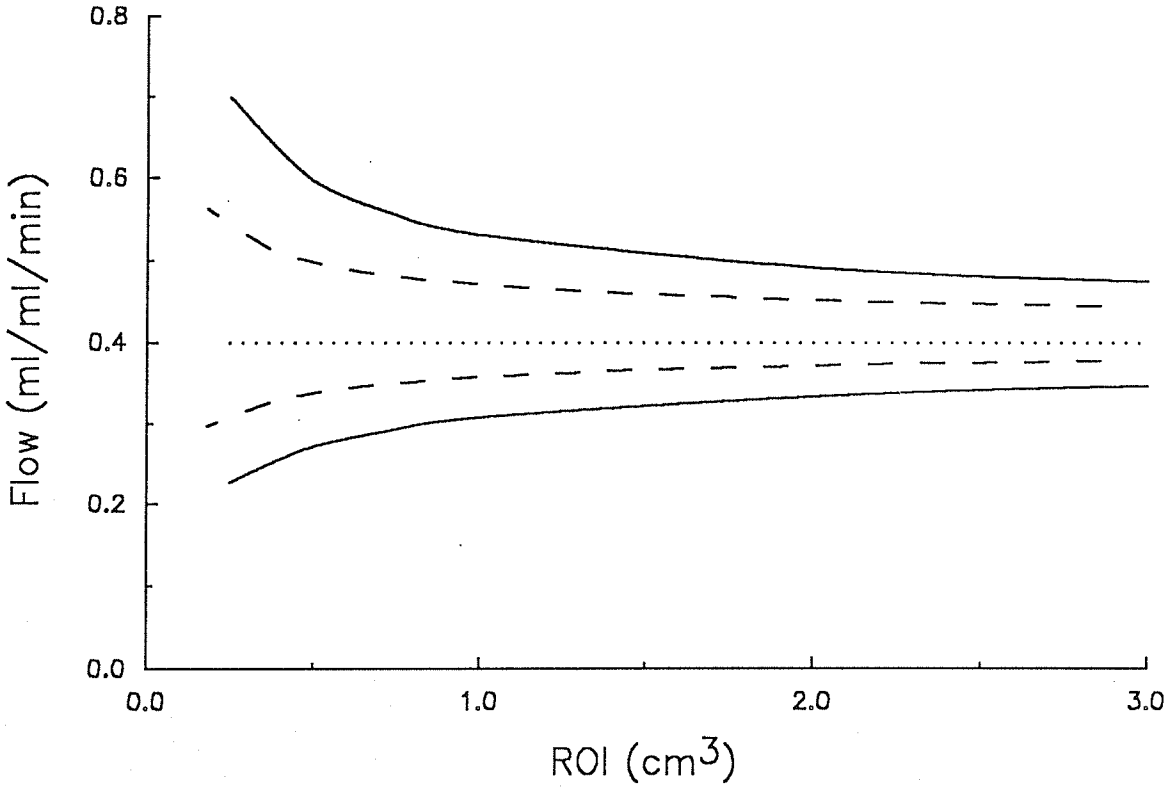
0.8
0.6
0.4
0.2
0.0
Flow (ml/ml/min)
0.0
1.0
2.0
3.0
ROI (cm3)

Table 1

The 5 and 95 percentiles from the grey matter flow distributions for a 2.0 cm^3 ROI and the following four scenarios:

(A) $C^{15}O_2$PET simulations with an activity concentration equal to 20 μCi/ml and a study duration equal to 6 minutes.

(B) $C^{15}O_2$PET simulations with a concentration equal to 30 μCi/ml and a 6 minute duration.

(C) $C^{15}O_2$PET simulations with a 30 μCi/ml concentration and a 4 minute duration.

(D) XeCT simulations with an inhaled xenon concentration of 33% and a study duration of 6 minutes.

Case	Percentiles		Spread	Difference in Spreads	
	5	95	(95-5)	From A	From D
A	0.666	0.960	0.294	-	+48%
B	0.689	0.929	0.240	-18%	+18%
C	0.629	1.011	0.382	+30%	+93%
D	0.710	0.908	0.198	-33%	-

Table 2

(A) The 5 and 95 percentiles from the $C^{15}O_2$PET simulations for grey matter, a ROI equal to 2.0 cm^3 and two scanning protocols.

(B) The 5 and 95 percentiles from the XeCT simulations for grey matter, a ROI equal to 2.0 cm^3 and two scanning protocols.

(A)

Scanning Protocol	Percentiles 5	95	Spread (95-5)	Increase in Spread from 7 to 19 scans
19 scans	0.666	0.960	0.294	
7 scans	0.601	1.080	0.479	39%

(B)

Scanning Protocol	Percentiles 5	95	Spread (95-5)	Increase in Spread from 7 to 19 scans
19 scans	0.721	0.892	0.171	
7 scans	0.710	0.908	0.198	14%

3.5 Discussion

Flow estimates from the XeCT simulations for both grey and white matter are more precise than those obtained from the $C^{15}O_2$PET simulations, as evident from the results illustrated in figures 7(a) and (b). These figures show the spread of the flow distribution to be narrower for the XeCT simulations than for the $C^{15}O_2$PET simulations over the entire ROI range studied. The narrower the spread of the flow distribution becomes, the greater the probability of obtaining the correct flow value. Before discussing the factors contributing to these results, dose calculations for both techniques is given, the importance of which will be evident shortly.

The relative radiation dose delivered to a patient by different diagnostic imaging modilities that use ionizing radiation is best defined using the concept of the Effective Dose Equivalent, H_E [Huda et al, 89a]. The Effective Dose Equivalent is defined as:

$$H_E = \sum w_T H_T \qquad (21)$$

where H_T is the dose equivalent in a given organ or tissue, T, and w_T is a weighting factor for organ T expressing the risk associated to radiation exposure to that organ. For a CT head scan, the H_E is 0.21 mSv obtained on a GE9800 scanner with the following technique factors: slice thickness equal to 10 mm, 120 kVp and 340 mAs [Huda et al, 89B]. With XeCT, seven scans were obtained with a corresponding H_E of 1.5 mSv. The H_E value for a one hour $C^{15}O_2$ inhalation PET

study, is 9.4 mSv, if the total activity administered was 9250 mBq [Huda et al, 90]. In this chapter, the $C^{15}O_2$ inhalation procedure used an administered activity of 1554 MBq. This factor is based on the assumption that a concentration of 20μCi/ml was inhaled at an absorbed rate of 350 ml/min (this rate includes the effect of the patient's dead space) for a duration of 6 minutes. The H_E for the $C^{15}O_2$PET technique is calculated to be 1.6 mSv. Notice, the effective dose equivalents received by a patient from the two techniques are approximately the same. This fact will be used as a 'yardstick' to evaluate any proposed alterations to improve the precision of either technique.

As mentioned in section 3.3, SNR in the serial scans will be the main factor determining the precision of flow estimates generated from either technique. In appendix II, parts (A) and (B), the SNR is calculated for measurements on grey matter with a 2.0 cm^3 ROI in both a XeCT and $C^{15}O_2$PET study. The SNR is given for all six enhanced CT images and the corresponding PET images from the $C^{15}O_2$PET scanning protocol. These results demonstrate that the SNR for every CT measurements is approximately three times greater than that for the corresponding PET measurements. Although not shown in the appendix, this ratio was found to be true for all ROI sizes. It is this significant difference between the SNR of the measurements used by the two techniques that is responsible for XeCT producing more precise flow estimates than those obtained from $C^{15}O_2$PET.

A simple method for increasing the SNR in the PET images is to increase

the concentration of $C^{15}O_2$ administered to the patient. Table 1 shows the improvement in flow estimates when the concentration of $C^{15}O_2$ inhaled is increased from 20μCi/ml to 30 μCi/ml. The SNR for the $C^{15}O_2$PET measurements on grey matter, with a 2.0 cm^3 ROI and an inhaled $C^{15}O_2$ concentration of 30 μCi/ml is given in appendix II, part (C). The SNR increased with the increased $C^{15}O_2$ concentration, resulting in an 18% decrease in the spread of the $C^{15}O_2$PET flow distribution.

Increasing the activity concentration administered will increase the radiation dosage delivered to the patient. For an activity concentration of 30μCi/ml, the H_E associated with the $C^{15}O_2$PET technique is 2.4 mSv, an increase of 50% from the H_E value for a concentration of 20μCi/ml. The $C^{15}O_2$PET simulations were also run with a concentration of 30μCi/ml, a study duration limited to 4 minutes and 19 scans. This high dose rate, short duration protocol had an associated patient dose of 1.6 mSv, identical to that of the 6 minute, 20μCi/ml study. Unfortunately, as evident from the results listed in table 1, the precision of the flow estimates actually decreased. In order to understand this trend, recall that flow is the product of two variables: k and l. For l to be determined precisely it is important that the tissue concentration of the tracer be sampled at saturation [Bews et al, 90]. From figure 2, the four minute mark corresponds to the onset of saturation in grey matter. If the study duration is only 4 minutes, saturation is not adequately sampled and λ will not be determined precisely. Since rCBF is a function of λ, the precision of its estimate,

in turn, will suffer.

In conclusion, it is evident that the precision of flow estimates will be improved if the concentration of $C^{15}O_2$ administered is increased and the study duration remains sufficiently long. The trade off is an increase in patient radiation dose. However, if the radiation dose delivered is to remain approximately equal to that of the XeCT technique, then increasing the $C^{15}O_2$ concentration is not a viable option since the study duration must be reduced to compensate for the increased activity. This reduction in study duration will lead to a significant decrease in the accuracy of results.

The infuence of image noise on the precision of flow measurements is affected by the scanning protocol chosen. Generally, the more scans acquired, the better the characterization of the tissue buildup curve and the more precise the flow measurements. The results presented in Table 2 reinforce this statement. With either technique, simulations run with the higher number of scans (ie. 18 for XeCT and 19 for $C^{15}O_2$PET) generated more precise flow estimates. However, in clinical practice, the number of scans used in the XeCT technique is usually limited to six or less, so as to minimize the radiation dose delivered to the patient. If 18 scans were actually used in practice, patient dose would be three times greater. This increase would be hard to justify as the results in Table 2 indicate only a 14% improvement in precision. For the $C^{15}O_2$PET technique, radiation dose is entirely independent of the number of scans acquired. The number of scans is restricted only out of a necessity to ensure a reasonable count rate in each.

Judging by the significant increase in the precision of the flow estimates when the number of scans was increased from seven to nineteen, optimization of the scanning protocol with the $C^{15}O_2$PET technique is essential.

Although every effort was made to make the comparison of the XeCT and $C^{15}O_2$PET techniques as fair as possible there are a few points which should be considered when assessing the validity of the results presented here.

Firstly, experimental data were used to quantify the magnitude of noise in a CT scan, while for PET the noise was calculated using a theoretical expression (equation 20). As such, there may be some doubt as to whether this formula effectively describes the noise in the images used in the actual $C^{15}O_2$PET clinical studies. In the original article describing the $C^{15}O_2$PET technique [Lammertsma et al, 89], the error in the clinical flow measurements for grey matter with a ROI of 4 cm^3 was approximately 6%, only a factor of 2 less than that found through computer simulations (computer simulations yielded an error of 12% for grey matter with a ROI of 4 cm^3). Although the precise definition of the error associated with the clinical measurements in the Lammertsma paper is not known, the similarity between the experimental and theoretical errors would suggest that the results generated by the simulations are reasonable.

Secondly, this study assumed that the noise in both CT and PET images are uncorrelated. However, in practise the noise is correlated, which results in the magnitude of the noise in a ROI depending on the shape of the ROI. A more precise account of the noise would include the correlation.

Thirdly, the only source of error analyzed in this study was noise. For a more thorough investigation, other potential sources of error associated with the two techniques should be considered. An outline of the most common sources of error is given in section 2.4.

Finally, the scanning protocols used by the two techniques have not been optimised (ie. the study duration, number of scans, etc.). Such optimization could potentially improve the results generated from either technique.

3.6 Conclusion

From the results generated in this study, it would appear that the precision of the blood flow measurements produced by the two techniques are similar. Considering the abundance of CT scanners as compared to PET scanners in hospitals, these results seem to favour the use of the XeCT technique. As well, the XeCT technique is much easier to apply. For instance, the concentration of the tracer in arterial blood must be determined in both techniques. For XeCT, this task is easily performed using a thermoconductivity analyzer, making it a completely non-invasive technique (section 2.3.3). With the $C^{15}O_2$PET technique, a complicated counting apparatus is required (section 2.3.3) and a catheter must be inserted into a radial artery [Lammertsma et al, 89].

However, the $C^{5}O_2$PET technique does offer some advantages. For instance, the precision of the rCBF measurements can be easily improved by increasing the concentration of the $C^{15}O_2$ administered to the patient (at the

expensive of patient radiation dose). With the XeCT technique, increasing the concentration of xenon inhaled is not a viable option considering the side-effects of xenon. Another advantage with PET is other physiological parameters such as cerebral blood volume and cerebral metabolism can also be measured. CT is much more limited in its functional imaging.

As a final remark, it should be remembered that there are many different PET based techniques for measuring rCBF (section 1.3), each with its own advantages and disadvantages. The $C^{15}O_2$PET technique was chosen for comparison with the XeCT technique because of the remarkable similarities between the two.

Chapter 4

The Expired Air Scanning Technique

4.1 Introduction

The measurement of regional cerebral blood flow, rCBF, using xenon enhanced computed tomography (XeCT) requires that the temporal buildup of xenon in cerebral tissue and arterial blood be determined (section 2.3). The arterial concentration of xenon is usually monitored indirectly by measuring the concentration of xenon in end-tidal air, which is assumed to be in equilibrium with the arterial concentration [Obrist et al, 67], with either a mass spectrometer or a thermoconductivity analyzer [Gur et al, 84].

The purpose of this chapter is to outline an alternative method for measuring the end-tidal concentration, one which uses the CT scanner to monitor the xenon concentration in expired air in conjunction with the buildup of xenon in brain tissue. The proposed technique, which shall be referred to as the expired air scanning technique, greatly simplifies rCBF measurements by eliminating the need for a specialized instrument to measure the xenon concentration in expired air.

4.2 Description of Technique

As previously mentioned, in a conventional XeCT rCBF study, the concentration of xenon in expired air is usually monitored with a thermoconductivity analyzer. The output from the analyzer is fed to a chart recorder to yield a continuous temporal plot of the xenon concentration over the entire length of the study. Figure 8 shows a theoretical expired air curve where

the rise of the curve represents inhalation and the fall of the curve represents exhalation. The end-tidal concentration is represented by the solid line through the troughs at the end of each exhalation.

The expired air scanning technique uses the CT scanner to measure the concentration of xenon in the patient's exhaled air, thereby eliminating the need for a thermoconductivity analyzer. With this approach the expired air is channeled alongside the patient's head and through the scan field via a flexible plastic tube (figure 9). A CT image acquired using this geometry will include a cross sectional view of both the head and the expired air tube. The CT number for the air in the tube image will be dependent on the concentration of xenon in the expired air and hence, serve as an indirect method of monitoring arterial xenon concentration.

During the course of a XeCT study, two or three baseline scans (scans taken prior to administration of xenon) and a series of enhanced scans (scans taken during the inhalation of xenon) are collected. The enhancement in CT number in the latter images will provide information on the temporal buildup of xenon in brain tissue. With the expired air tube properly positioned in the scan field, each of the images will also convey information pertaining to the xenon concentration in expired air at selected times during the study. Provided the relationship between the xenon concentration in expired air and CT number

Figure 8

The theoretical expired air curve (solid line) that would be recorded by a thermoconductivity analyzer during the course of a XeCT study. The rise of the curve represents inhalation and the fall of the curve represents exhalation.

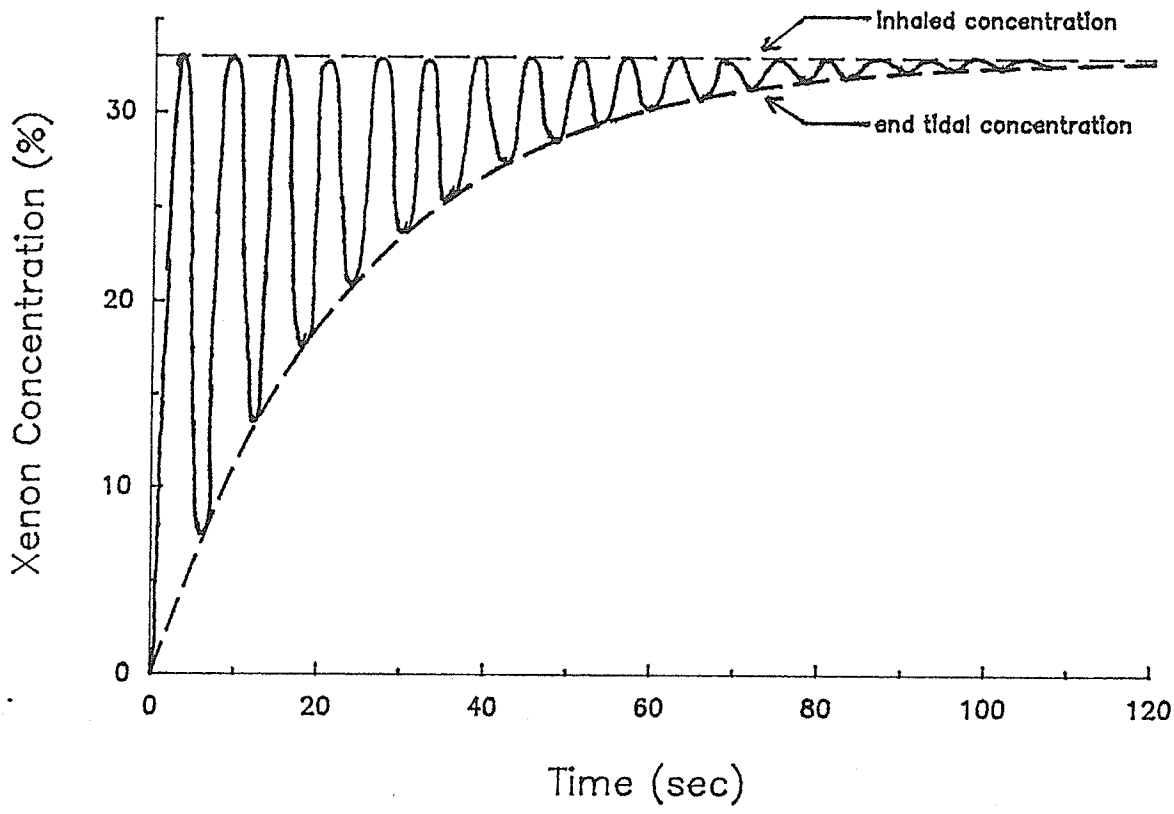
Inhaled concentration
end tidal concentration
Xenon Concentration (%)
30
20
10
0
0
20
40
60
80
100
120
Time (sec)

Figure 9

A schematic diagram of the expired air scanning technique. The cutoff of the patient's head and of the expired air tube represents the CT image that would be acquired.

Inhaled Xenon/Air Mixture

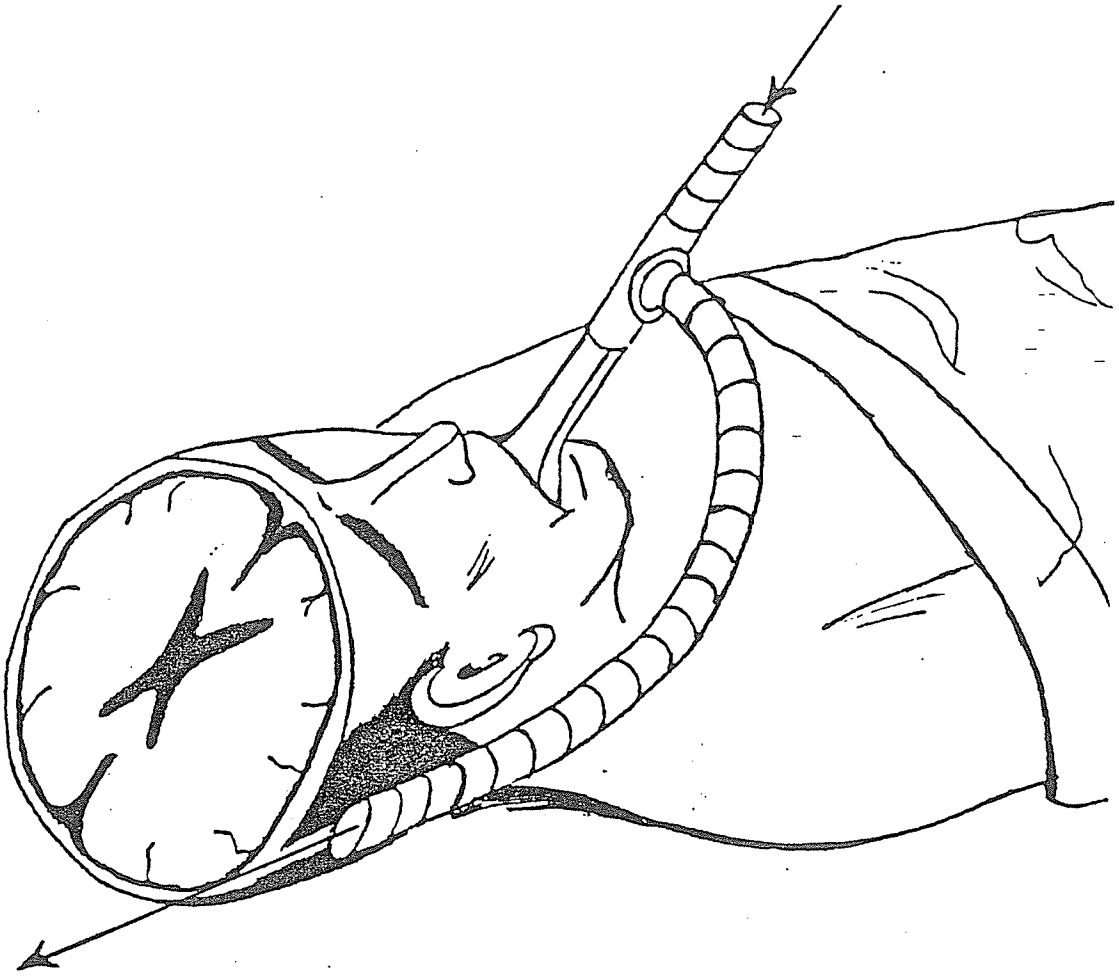

Exhaled Air

is known, the enhancement in CT number of the expired air in each of the serial scans can be converted into a corresponding concentration of xenon.

Recall from chapter 2 that a single exponential function (equation 14), referred to as the breathing curve equation, is fit to the end tidal xenon concentration data to generate values for the breathing curve rate constant, b, and the xenon saturation concentration C_{max}. This approach simplifies the Kety equation (equation 15), which in turn, is fit to the tissue buildup data to generate estimates of the rate constant k and the partition coefficient, λ. rCBF is the product of these two parameters. With the expired air scanning technique, estimates of b and C_{max} are generated by fitting the breathing curve equation to the xenon concentration data obtained from the enhanced scans of the expired air tube.

The expired air scanning technique samples the expired air with no regard as to the patient's breathing cycle. As a result, the end-tidal concentration may not neccessarily be sampled. The inability of the expired air scanning technique to ensure that the end-tidal expired air is sampled will introduce error into the fitted values of b and Cmax, and in turn rCBF. The purpose of this chapter is to determine the magnitude of this error and thus the feasibility of the expired air scanning technique.

4.3 Relationship between the xenon concentration in air and CT Number

In order to implement the expired air scanning technique, the relationship

between the xenon concentration in exhaled gas and corresponding CT number must be determined. It is assumed that the relationship is linear and has the following form:

$$HU = \Omega C + HU_{air}, \qquad (22)$$

where HU is the measured CT number of the expired air, C is the concentration of xenon in air, HU_{air} is the CT number for air and Ω is the calibration factor.

Method

The following experiment was carried out to determine the calibration factor, Ω, relating xenon concentration in an air mixture to CT number. The apparatus for this experiment consisted of one head phantom, four plastic syringes filled with different concentrations of xenon in air (0, 11, 22 and 33%) and a CT scanner. The syringes were attached to the head phantom at four marked locations and the phantom was placed in the scan field of the CT scanner, figure (10). Four scans of the phantom were acquired in order to obtain a mean CT number and a standard deviation for each concentration. To determine if Ω is position dependent, the syringes' positions were interchanged and the procedure repeated for each permutation. The CT scan technique factors used were a 10 mm slice thickness, 2 sec scan time, 120 kVp and 200 mA.

Results

The experimentally determined calibration factors, Ω, for the four different

position on the head phantom along with the corresponding CT numbers for air are presented in table 3. The relationship between xenon concentration in air and corresponding CT number is plotted in figure (11).

Figure 10

Diagram of the head phantom with attached xenon filled syringes placed in the scan field. The scan field is represented by the dashed lines.

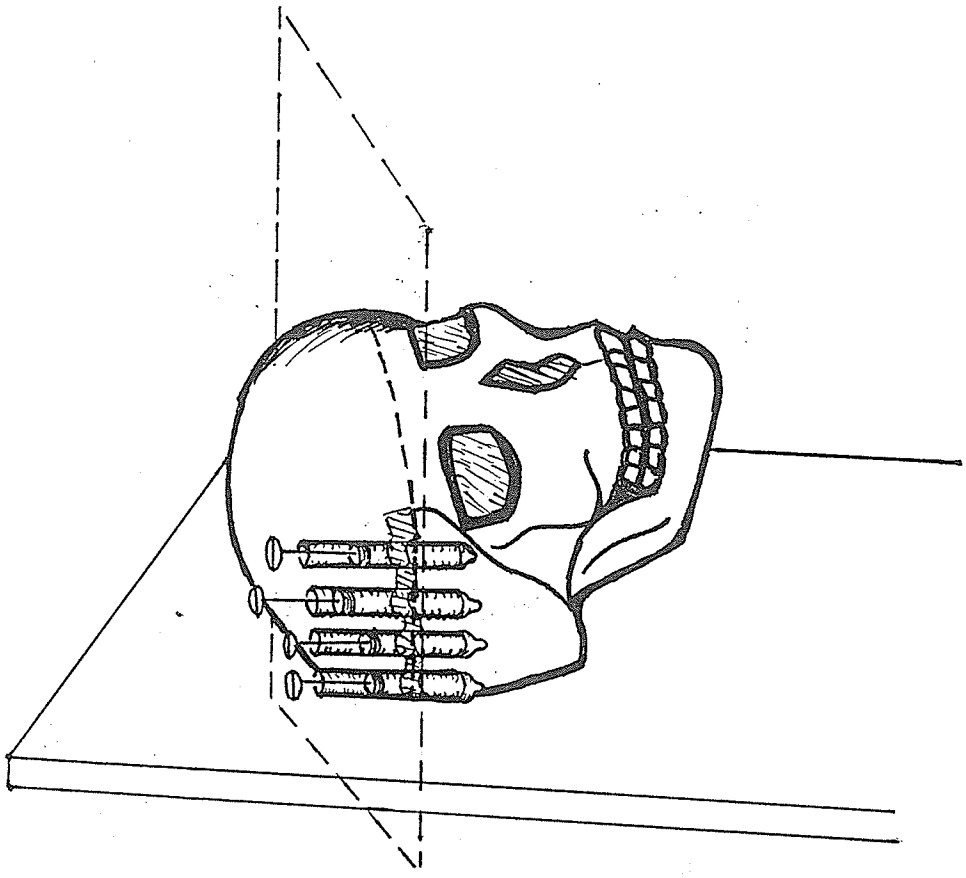

Table 3

The calibration factor relating CT number to xenon concentration in air and the average CT number for air at four locations on the head phantom.

Position Number	Calibration Factor (HU/ml/ml)	CT Number for air (HU)
1	0.64 ± 0.01	-1000.2 ± 0.4
2	0.61 ± 0.01	-1000.6 ± 0.2
3	0.63 ± 0.01	-1006.8 ± 0.9
4	0.64 ± 0.01	-1010.7 ± 0.9

Figure 11

CT number versus concentration of xenon in air. Each line represents one of four positions on the head phantom.

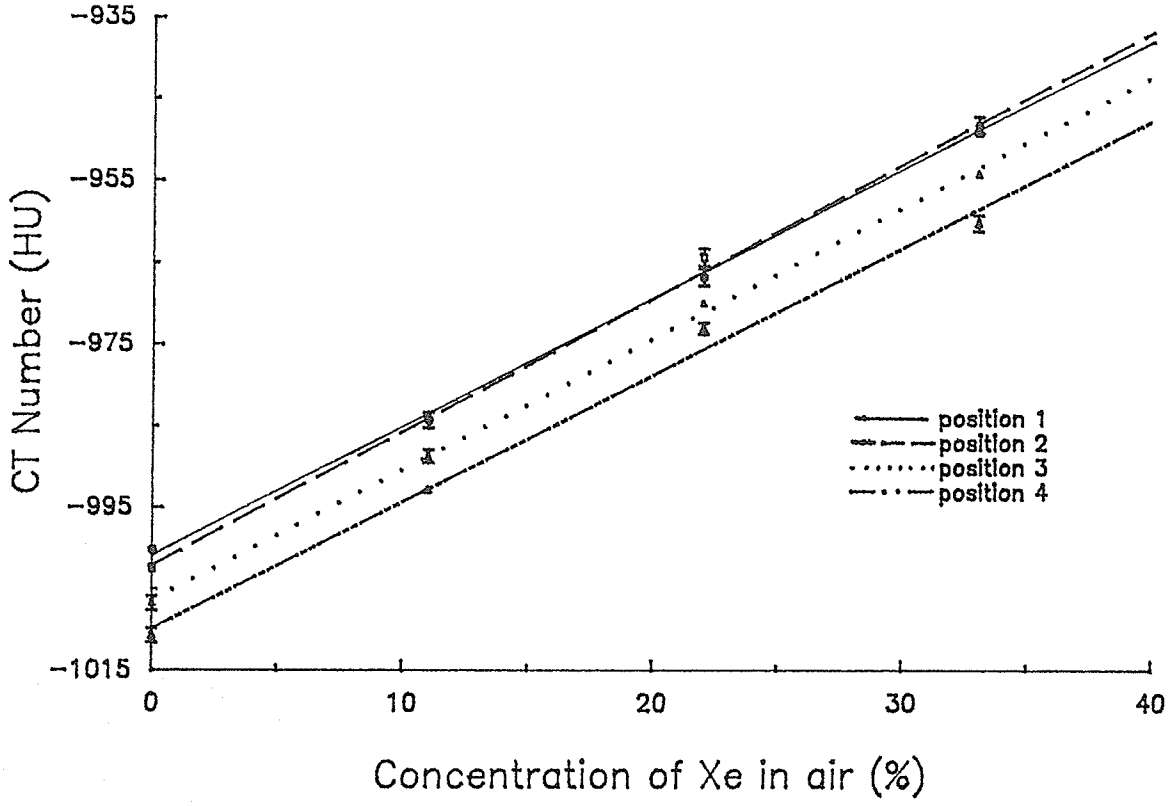
−935
−955
−975
−995
−1015
CT Number (HU)
0
10
20
30
40
Concentration of Xe in air (%)
position 1
position 2
position 3
position 4

Discussion

The experimental data plotted in figure 11 indicates that the CT scanner is able to detect changes in xenon concentration in air for concentrations of xenon typically found in a clinical rCBF study. As well, the results shown in figure 11 verify that the relationship between the xenon concentration in air and CT number is linear. However, the results also indicate that CT_{air} is position dependent, which implies that in a clinical study the expired air tube must remain in a fixed position throughout the procedure.

In a XeCT study, the CT numbers for two concentrations of xenon are always known; the 0% (baseline scan) and 33% (scans at saturation level). Since the relationship is linear, these two data points will be sufficient to determine the calibration factor and thus, the proposed technique is self-calibrating.

4.3.1 The Effect of Error in the Calibration Factor on the Accuracy of rCBF Measurements

To determine the effect of measurement errors in the calibration factor, Ω, on the accuracy of calculated rCBF values, the following study was performed.

Method

The computer simulation described in appendix III was used to generate theoretical tissue buildup curve data using the following parameters: a two second scan time, two baseline scans and five enhanced scans taken at 45 second intervals, a theoretical breathing curve rate constant and saturation level of 2.5

min^{-1} and 33% respectively, a correct calibration factor of 0.63 HU/ml/ml, a partition coefficient equal to 0.8 ml/ml and a rate constant equal to 1.0 min^{-1}. The Kety equation was then refit to this data using the correct breathing curve rate constant and saturation level but a calibration factor one and two standard deviations, σ, (as determined in the phantom study) removed from the input value to yield best fit estimates of k and λ (and hence rCBF) in the presence of calibration factor errors.

Results

The errors in rCBF arising as a result of inaccuracies in the calibration factor are presented in Table 4.

Table 4

The percent error in rCBF calculations as a result of using the incorrect calibration factor relating CT number to xenon concentration in air.

	Ω plus 1σ	Ω minus 1σ	Ω plus 2σ	Ω minus 2σ
% error in flow	1.4	1.5	2.9	3.0

Discussion

As evident from Table 4, errors in the calibration factor, Ω, will have little impact on the accuracy of rCBF estimates. Only a 3% error in flow was introduced when a calibration factor two standard deviations removed from its correct value was used in curve fitting.

4.4 Technical Factors Influencing the Precision and Accuracy of the Expired Air Scanning Technique

To determine the errors introduced in rCBF measurements as a result of implementing the expired air scanning technique, the following study was preformed.

Method

The computer simulation outlined in appendix III was run for the two types of brain tissue: white matter (rCBF = 0.4 ml/ml/min, λ = 1.4 ml/ml) and gray matter (rCBF = 0.8 ml/ml/min, λ = 0.8 ml/ml) [Good et al, 87b]. A total of 1000 runs were obtained for each tissue type. The theoretical input values for b and C_{max} used in the simulations were 2.5 min^{-1} and 33% respectively. A scanning protocol of two baseline scans and five enhanced scans at 45 second intervals was used. The simulations yielded distributions for the variables b, C_{max}, k, λ and rCBF. The spread of the latter distribution was used to quantify the errors introduced in the rCBF estimates as a result of using the expired air scanning

technique.

Results

The distribution for the breathing curve rate constant b (1000 simulations) is displayed in figure 12. The corresponding distributions of rCBF for grey and white matter are shown in figures 13 and 14 respectively.

Figure 12

The distribution of the breathing curve rate constant, b, estimates generated from 1000 runs of the expired air scanning technique simulation. The input value for b was 2.5 min^{-1}

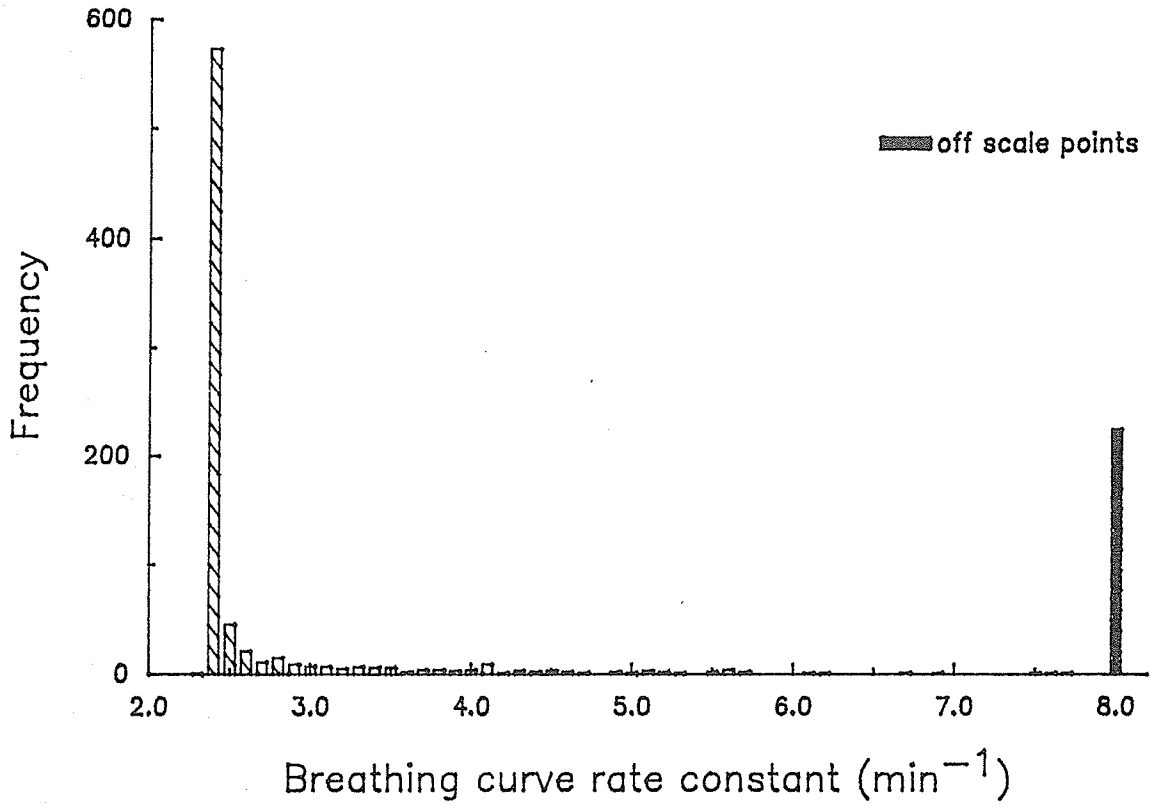
600
400
200
0
Frequency
off scale points
2.0
3.0
4.0
5.0
6.0
7.0
8.0
Breathing curve rate constant (min^{-1})

Figure 13

The distribution of grey matter flow estimates corresponding to the distribution of the breathing curve rate constant b shown in figure 12. The input flow value was 0.8 ml/ml/min

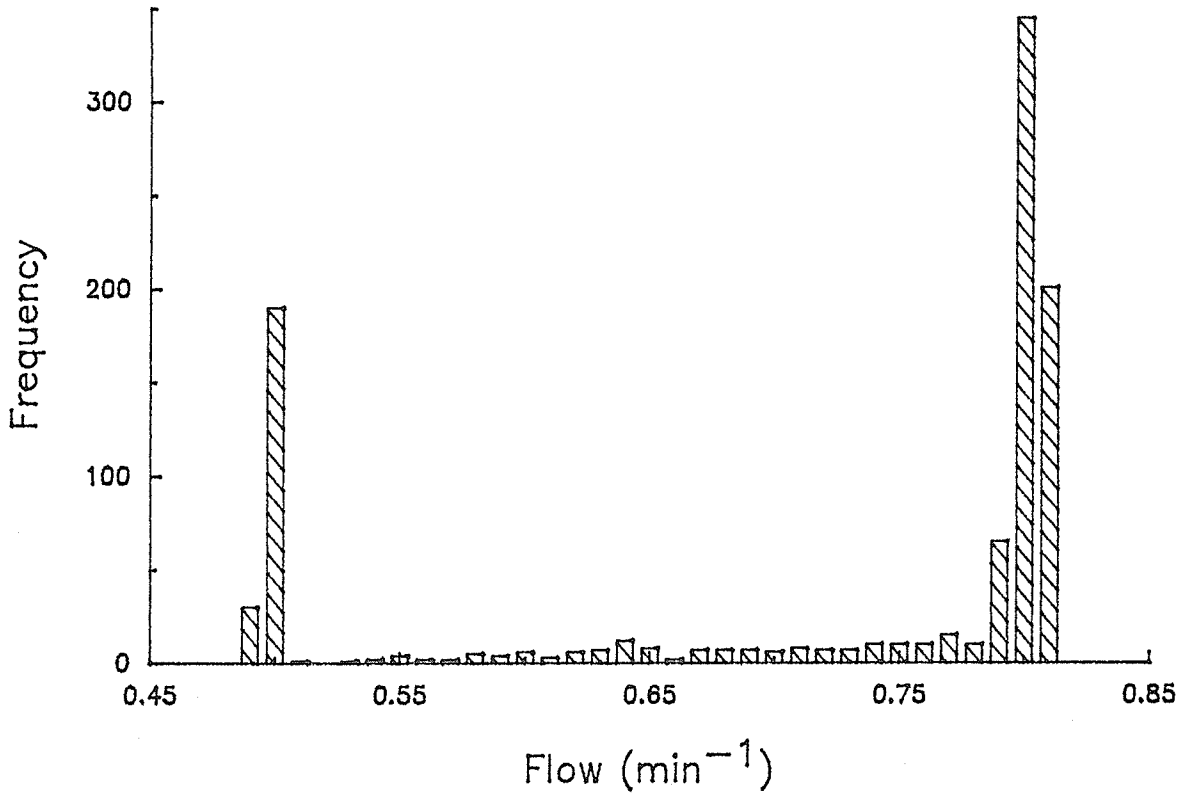
300
200
100
0
Frequency
0.45
0.55
0.65
0.75
0.85
Flow (min^{-1})

Figure 14

The distribution of white matter flow estimates corresponding to the distribution of the breathing curve rate constant b shown in figure 12. The input flow value was 0.4 ml/ml/min.

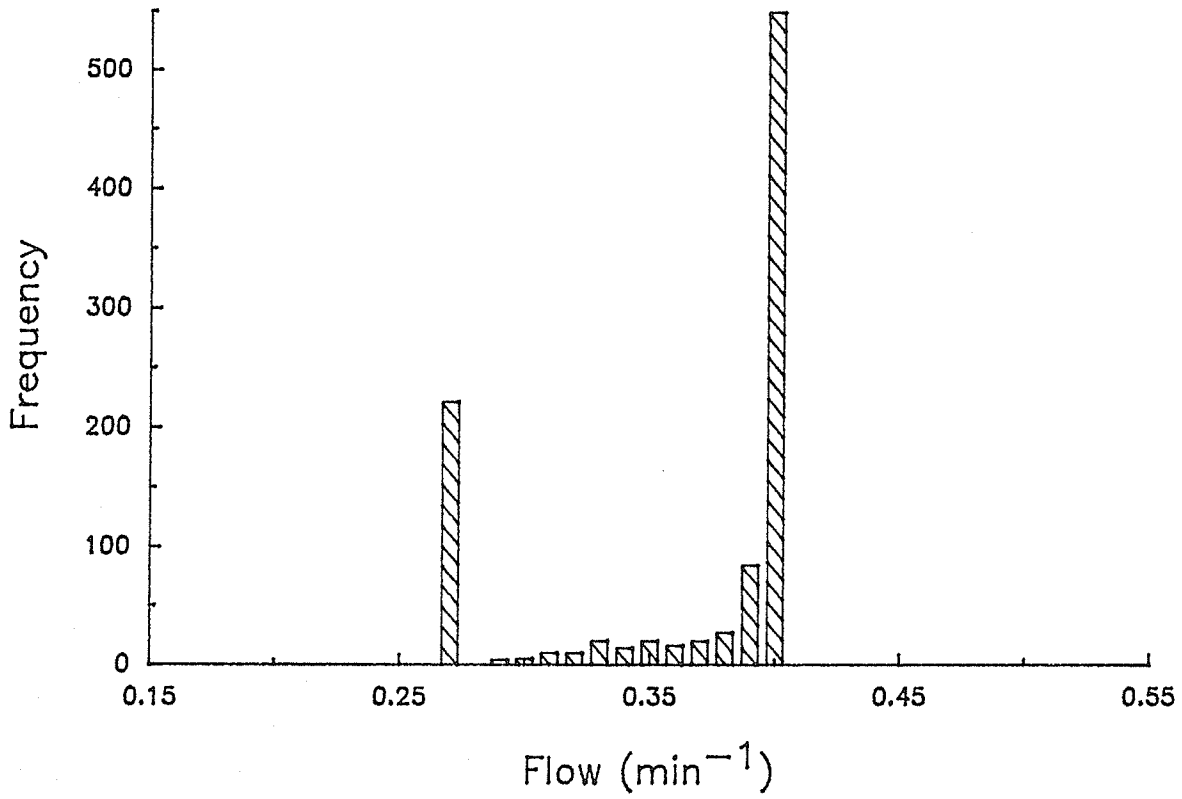
Frequency
500
400
300
200
100
0
0.15
0.25
0.35
0.45
0.55
Flow (min^{-1})

Discussion

For a breathing curve rate constant of 2.5 min^{-1}, saturation is reached after about one and a half minutes of xenon inhalation (see figure 8). The scanning protocol consists of scans every 45 seconds and as a result, only one scan was acquired on the rise of the breathing curve (ie. at 45 secs). The location of this one scan in the breathing cycle (see figure 20) will dominate over all of the other points in the determination of b. If the 45 second scan is taken during inhalation, the xenon concentration measured will correspond to the plateau following the last end tidal value just before the 45 second mark. In this case, the resulting rate constant estimate will be very close to the correct value, as evident from figure 13, where approximately 50% of the values of b are equal to 2.4 min^{-1}. However, if the 45 second scan is taken during exhalation, the concentration of xenon measured can range anywhere from the end tidal point to the saturation level. Since all possible xenon concentration values measured on this portion of the breathing curve are greater than the end-tidal value, b will always be overestimated with its specific value depending on where the scan falls between the two above mentioned boundaries.

Grey and white matter flow distributions both show two distinct peaks. The peak at the correct flow value is due to the large peak in the distribution for b at 2.4 min^{-1}. The second peak, representing underestimated values, is due to those simulations in which b is greatly overestimated. It has been shown that as b becomes increasingly overestimated the corresponding flow value will converge

to a particular underestimated value [Good et al, 87a].

The anomaly of having two distinct, widely separated peaks in the flow distribution makes quantifying the error, resulting from the implementation of the expired air scanning technique, difficult. Although it is possible to state that a particular flow measurement will fall within a given range, it is difficult to make any further predictions on the precision, due to the odd shape of the distribution. Fortunately, the duration of a CT scan will drastically change the shape and spread of the distribution of possible b values. The effect of the scan duration on the precision and accuracy of the expired air scanning technique is the topic of the next section.

The effect of incorrectly measuring b on the accuracy of rCBF estimates is more pronounced for high flow tissue (grey matter) than low flow tissue (white matter). As a result, unless otherwise mentioned, simulations in the following sections will deal strictly with the worse case only (ie. grey matter). As well, a C_{max} of 33%, a b of 2.5 min^{-1} and a scanning protocol consisting of 2 baseline scans and 5 enhanced scans, each separated by 45 seconds, will be used.

4.4.1 **Scan Duration**

The computer simulations run in the previous section assumed an instantaneous scan time. In practice, a CT scan is acquired in a finite amount of time, typically around 2 seconds. This factor will affect the expired air xenon

measurements. A person at rest typically takes about four seconds to complete a breath and as a result, the CT number for the image of the expired air tube will be averaged over a segment of the breathing cycle (figure 20). In other words, due to the time duration of a scan, it impossible to measure an instantaneous concentration of xenon in the breating cycle; for instance, an end tidal point.

Method

The computer simulation described in appendix III was modified to account for a finite scan duration by sampling the xenon concentration 64 times over a two second portion of the breathing curve and averaging all of the samples. To demonstrate the effect of different scan durations on flow measurements, simulations (1000 runs for each) were run for a series of scan times in the range 0 to 3 seconds.

Results

The distribution generated for rCBF from the simulation with a two second scan duration is shown in figure 15. The uncertainty in flow measurements (5 and 95 percentiles of the flow distribution) as a function of scan duration is illustrated in figure 16. The input rCBF value is represented by a dotted line.

Figure 15

Distribution of grey matter flow estimates for a 1000 runs of the expired air scanning technique with a two second scan duration. The imput flow value is 0.8 ml/ml/min.

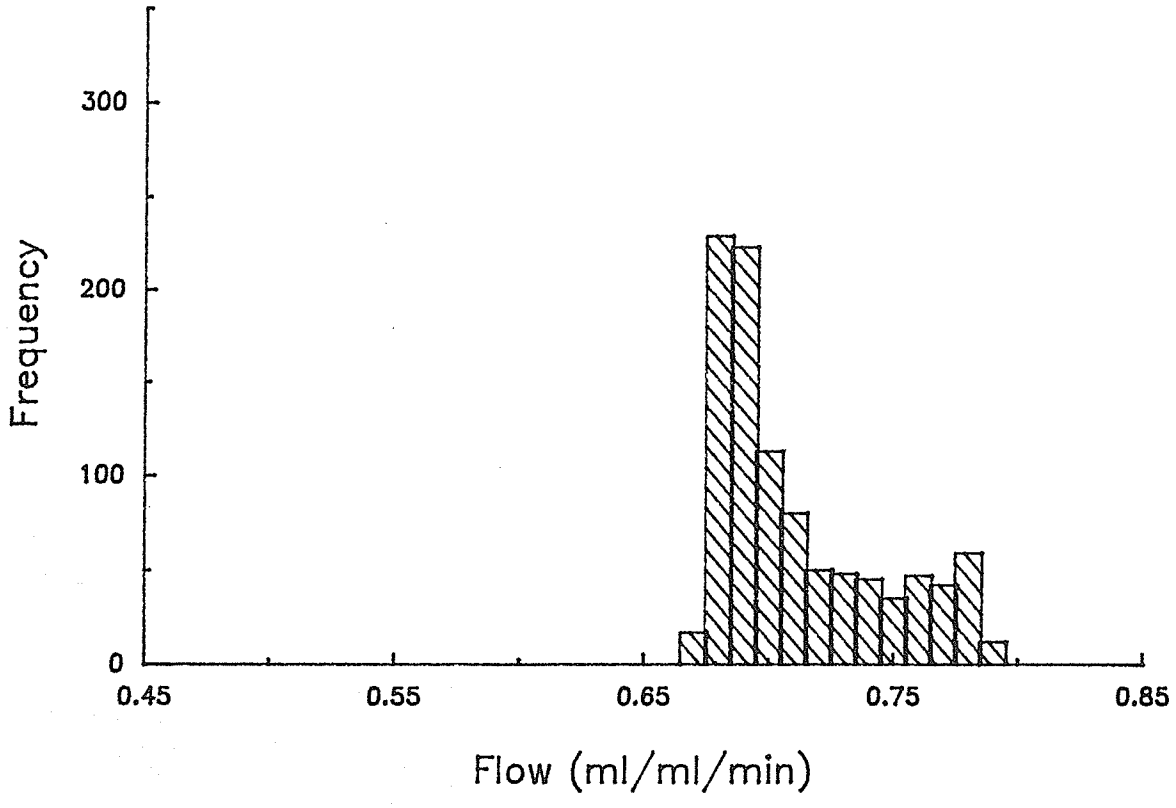
300
200
100
0
Frequency
0.45
0.55
0.65
0.75
0.85
Flow (ml/ml/min)

Figure 16

The error in a grey matter flow measurement due to the implimentation of expired air scanning as a function of scan duration. The 5 and 95 percentiles from the flow distribution are represented by dashed lines and the input flow value by a dotted line.

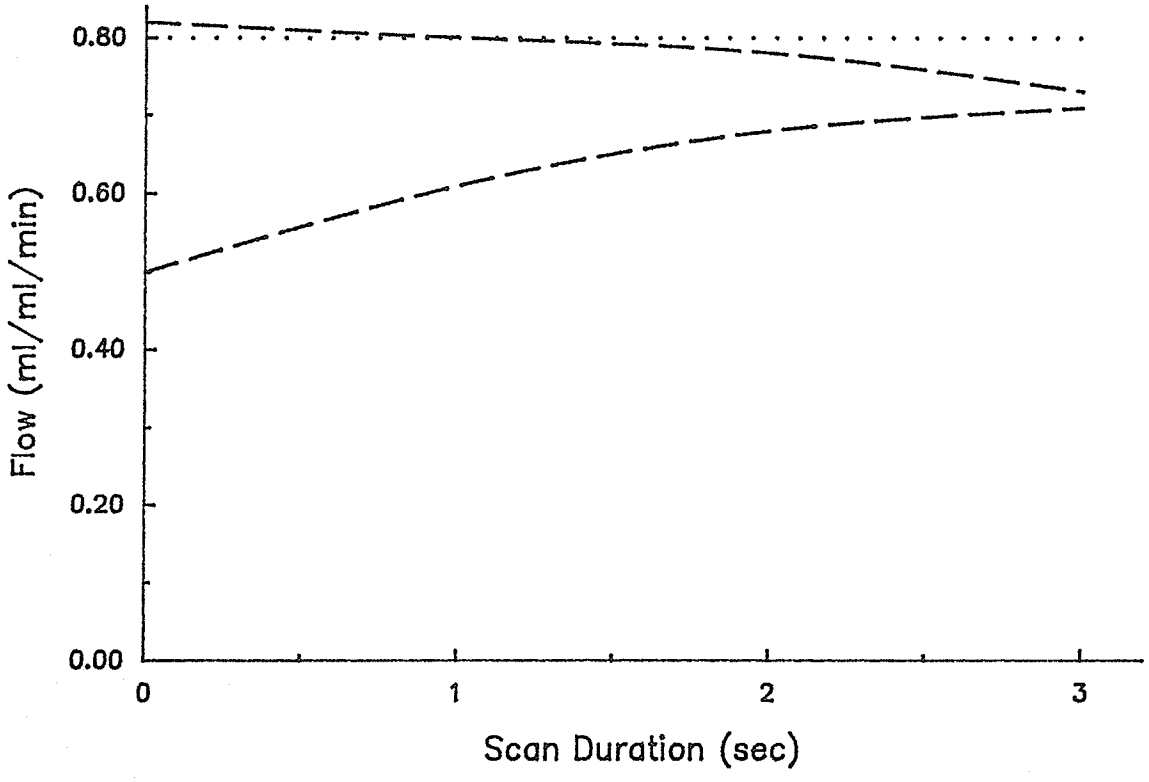
0.80
0.60
0.40
0.20
0.00
Flow (ml/ml/min)
0
1
2
3
Scan Duration (sec)

Discussion

The range of values for the concentration of xenon in exhaled air measured by the CT scanner is dependent on the scan duration. The longer the scan duration, the larger the segment of the breathing cycle that the xenon concentration measurement is averaged and the smaller the range of possible values for the xenon concentration that can be measured by the CT sanner. The largest range of possible xenon values extends from the end-tidal curve to the saturation level and corresponds to an instantaneous scan duration. As the scan duration increases this range decreases.

By reducing the range of xenon concentration values measured by the CT scanner, so too is the range of possible b values and in turn, the range of possible rCBF values generated by XeCT with expired air scanning. This relationship between scan duration and the spread in the rCBF distribution is seen by comparing figures 13 and 15. The spread associated with the rCBF distribution for the 2 second scan time is approximately 3 times smaller than that for an instantaneous scan time. In addition, the shape of the two distributions differ significantly. With a two second scan time, there is only one peak as opposed to the double peak associated with the instantaneous scan. The disappearance of the second peak with a 2 second scan duration is due to the elimination of the greatly overestimated values of b.

Figure 16 illustrates the decrease in the spread of the flow distribution as the scan duration increases. Notice as well, that as the scan duration increases,

the mean of the flow distribution shifts away from the input value. The accuracy of rCBF measurements depends on the ability of the CT scanner to measure the end-tidal concentration of xenon in exhaled air. However, the end-tidal concentration corresponds to one of extreme values in the range of possible xenon concentrations measurements and it is only possible to measure this value with a very short scan duration. For a longer scan duration, since it is impossible to measure the end-tidal concentration, it impossible to derive the correct rCBF value. In general, increasing the scan duration results in an improvement in precision, but at the expense of accuracy.

The simulations in the following sections will assume a scan duration of two seconds, which is typical of many modern CT scanners.

4.4.2 **Transit Volume**

In conventional XeCT studies, the thermoconductivity analyzer measures the xenon concentration at the patient's mouth. All computer simulations to this point have assumed that the expired air scanning technique was able to measure the xenon concentration at this location as well. However, this is not the case in practise. The xenon concentration can be measured only at the scan location which, in general, will be located some distance from the patient's mouth. Clearly, a time delay will be introduced as the expired gas travels that finite distance. The volume of the tube extending from the mouth to the scan field shall be referred to as the transit volume. The following simulations were performed

to study the effects of different sizes of the transit volumes.

Method

The computer simulation, outlined in appendix III, was modified to simulate varying transit volumes. The time delay due to the transit volume was calculated by assuming a rate of flow for exhaled air of 200ml/second [Green, 70], an expired air tube diameter of 2.1 cm and a tube length ranging from 0 to 40 cm. A 1000 simulations were run for each length of tube.

Results

The results of the transit volume simulations are presented in figure 18. The mean value of the flow distribution, represented by a solid line, is plotted as a function of transit volume. The flow distribution is seen to shift away from the correct value as this volume increases, indicating a slight reduction in measurment accuracy. Again, the input value is represented by a dotted line.

Figure 17

The error in grey matter flow estimates as a function of transit volume (ie. transit delay). The mean value of the flow distribution is represented by a solid line and the input value by a dotted line.

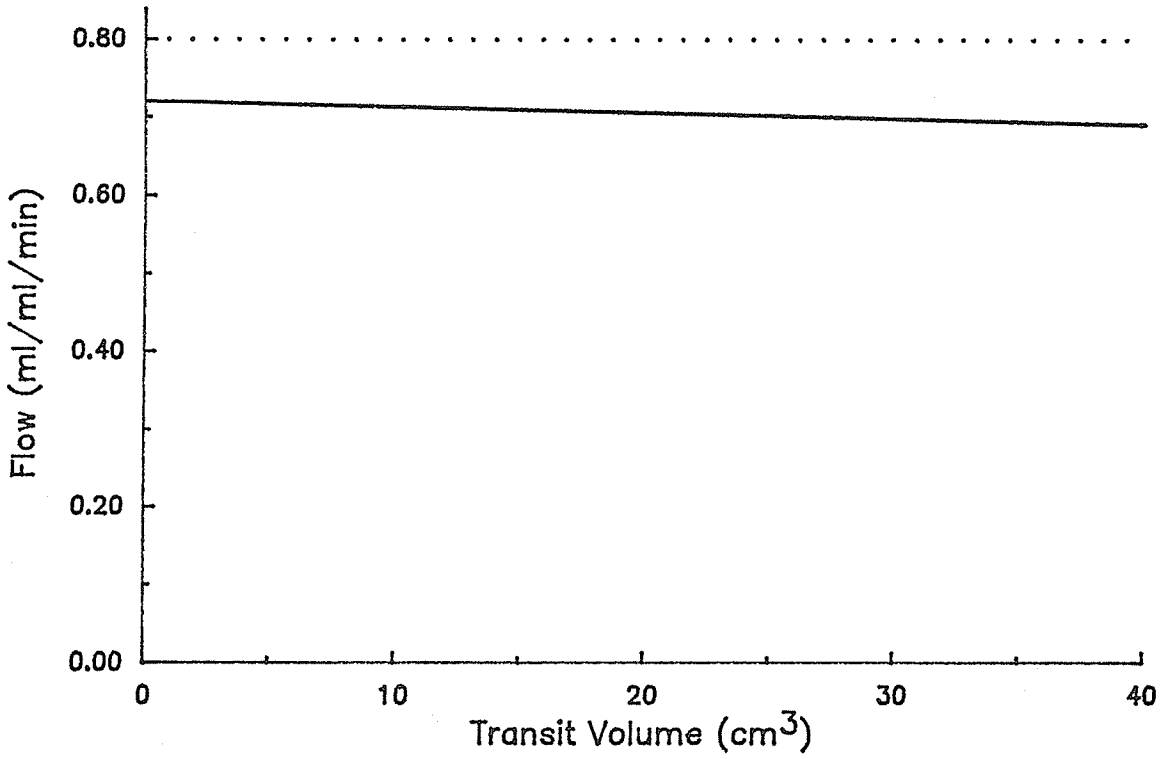
0.80
0.60
0.40
0.20
0.00
Flow (ml/ml/min)
0
10
20
30
40
Transit Volume (cm3)

Discussion

The volume of the expired air tube introduces a timing error when characterizing the breathing curve through CT scanning. The xenon concentration in expired air sampled in conjunction with brain tissue buildup, actually represents a data point at some time earlier that the scan time. However, judging by the results of the computer simulations, it would appear that the error introduced by the transit volume is quite small. For example, the mean flow value from the simulations with a 40 cm length tube is only 4% lower the mean value from the simulations with no transit volume.

The effect of the transit volume can be reduced by decreasing the diameter of the tube. Two conditions must be considered when choosing a particular tube diameter. Firstly, the tube must remain large enough so the patient can exhale comfortably and secondly it must also be of sufficient size to keep the effect of CT noise to a manageable level (section 4.4.3).

All computer simulations performed in the sections that follow will assume an expired air tube with a diameter of 2.1 cm and a length of 25 cm.

4.4.3 CT Noise in the Expired Air Tube Images

Statistical noise is present in all CT images. This noise will limit the ability to measure precisely the CT number corresponding to the xenon concentration in the expired air tube. The magnitude of the noise can be determined from the standard deviations associated with the CT numbers for the cross sectional images

of the syringes in section 4.3. Assuming these values to be similar to the standard deviation in the images of the expired air tube and knowing the area of the tube, the standard error for the expired air CT number measurements can be calculated.

The standard error associated with the images of the syringes, calculated using a ROI of 2.93 cm^2, was 0.18 HU. For a tube with a cross sectional area of 3.5 cm^2, corresponding to a diameter of 2.1 cm, the standard error would be about 0.15 HU. To determine the effect of CT noise of this magnitude, the following study was performed.

Method

The computer simulation outlined in appendix III was designed to examine the effect of CT noise in the images of the expired air tube. In this model, a random number generator with zero mean and unit variance was used to simulate CT noise. The output from the generator was multiplied by a number representing the variance of the CT noise and added to the simulated CT numbers, CT(t) and $CT(t)_{air}$ used to calculate the concentration of xenon in the expired air tube for a particular image. This procedure was repeated for each scan to generate a noisy breathing curve data set. Equation 14, was then fit to the noisy data set to generate best fit estimates of b and C_{max}. The Kety equation was then used to generate estimates of k and λ in the presence of CT noise in the breathing curve. Results were generated for CT noise characterized by a standard error ranging between 0 and 0.3 HU. One thousand simulations were run for

each particular magnitude of CT noise.

Results

The uncertainty in rCBF measurements is shown in figure 18 as a function of the magnitude of CT noise in the images of the expired air tube. The 5 and 95 percentiles from the rCBF distribution are represented by dashed lines and the input value by a dotted line.

Figure 18

Error in flow measurements as a result of CT noise in the expired air tube images. The 5 and 95 percentiles are represented by dashed lines and the correct value by a dotted line.

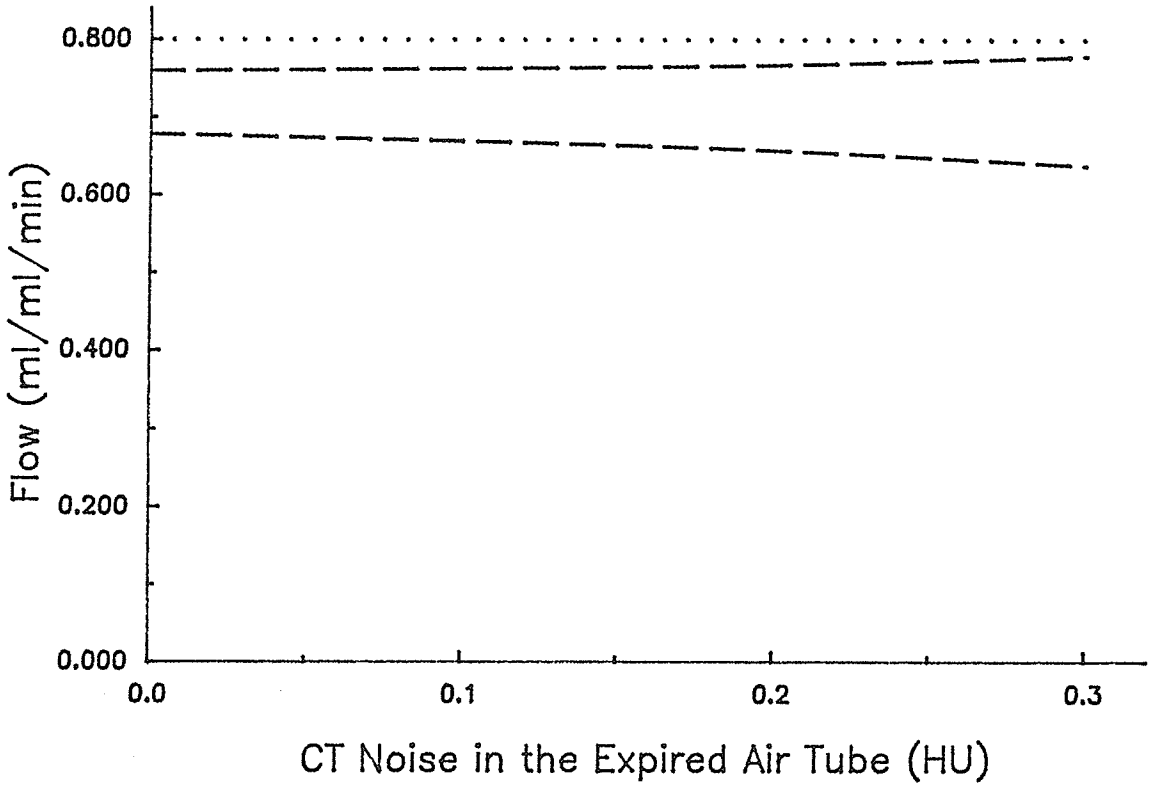
0.800
0.600
0.400
0.200
0.000
Flow (ml/ml/min)
0.0
0.1
0.2
0.3
CT Noise in the Expired Air Tube (HU)

Discussion

CT noise has the effect of increasing the uncertainty in flow measurements. However, judging from the results presented in figure 18, the effect is relatively small provided the magnitude of noise is within the range studied here. A tube similar in diameter to the one described earlier (2 cm) should limit CT noise to within this range. In general, to limit the effect of CT noise, the cross sectional area of the expired air tube should be as large as possible so that the noise can be reduced through pixel averaging. However, the trade off with increasing the tube diameter is the effect of the transit volume will increase.

In the following simulations, it is assumed that noise characterized by a standard error of 0.15 HU, will be present in all images of the expired air tube.

4.4.4 Data Collection Protocol

The scanning protocol used in the previous simulations, produced only a few data points on the rise of the breathing curve, as discussed at the beginning of section 4.4. Inadequate sampling on the rise of the breathing curve can result in a large uncertainty in the derived value of the breathing curve rate constant, b. If more scans were obtained on the rise of the curve, the curve would be better characterized and the uncertainty in b would decrease. To assess the potential of decreasing the error in b by increasing the number of enhanced scans acquired, the following study was performed.

Method

Simulations were run for the scanning protocol describe previously, with additional scans in the first minute of inhalation. Three alterations to the protocol were examined: one additional scan at 60 seconds; two additional scans at 30 and 60 seconds; and three additional scans at 15, 30 and 60 seconds. A 1000 runs were completed for each alteration.

Results

As stated above, the error in blood flow is characterized by the spread of the distribution generated by the simulations. In table 5, the spread of the rCBF distribution, defined as the difference between the 5 and 95 percentiles, is given for the standard protocol and the three alterations described above. Also included in Table 5, is the percent decrease in the spread as the number of enhanced scans increases.

Table 5

The spread of the flow distribution for the standard protocol and three alterations: 1 additional scan at 60 seconds, 2 additional scans at 30 and 60 seconds, and 3 additional scans at 15, 30 and 60 seconds. The percent decrease in the spread of the flow distribution as the number of additional scans is also presented.

	standard protocol	additional scans (seconds) 1 (60)	2 (30, 60)	3 (15, 30, 60)
spread (95% - 5%) ml/ml/min	0.133	0.118	0.116	0.115
Percent decrease	-	11.3	12.8	13.5

Discussion

The greatest improvement in precision of rCBF estimates occurred with the addition of one scan at 60 seconds. Additional scans at 15 and 30 seconds showed only a slight improvement. This lack of improvement with additional scans at 15 and 30 seconds is due to the large difference between the end-tidal curve and the saturation concentration value at these times compared to that at 60 seconds. As discussed in section 4.4.1, the larger this spread, the greater the range of possible measured values for the xenon concentration in the expired air tube. This in turn, leads to an increase in the uncertainty in b and rCBF.

These results suggest that additional scans near the end of the rise of the breathing curve have the greatest effect on rCBF precision. However, in clinical practice it is not known a priori how fast the breathing curve rises to saturation and therefore it is difficult to choose the optimal scanning times. To ensure the breathing curve is properly characterized as many scans as possible should be obtained in the first minute of xenon inhalation. Clearly, the necessity of keeping patient dose below an acceptable level will restrict the number of scans acquired.

4.5 Evaluation of the Expired Air Scanning Technique

Statistical noise is present in all CT images and it has been determined that the presence of this noise in the head images used to monitor xenon buildup in tissue is one of the dominant sources of error in the XeCT technique [Good et al, 87b]. The relative importance of the errors introduced in rCBF estimates due to

the expired air scanning technique were examined through comparison with these errors. CT noise in tissue buildup images has previously been studied using Monte Carlo simulations by Bews et al [Bews et al, 90].

Method

The Monte Carlo computer simulations used to quantify the error in rCBF due to CT noise in tissue buildup images are described in chapter 3.2. Briefly, the Kety equation (equation 15) was fit to a noisy set of data extracted from the enhanced images to generate 'best fit' estimates of k and λ. rCBF was calculated as the product of these two parameters. This procedure was repeated 1000 times to generate a distribution of rCBF values for a particular magnitude of CT noise. For these simulations, theoretical values of 2.5 min^{-1} and 33% were used for b and C_{max}, respectively.

To study the combined effect of the expired air scanning technique and CT noise in the buildup images, on the accuracy of rCBF estimates, the computer program designed to simulate the expired air scanning technique was combined with the CT noise program. The first step in a single run of this combined program consisted of generating values of b and C_{max} from the simulation of the expired air scanning technique. Next, a noisy tissue buildup data set was generated using the CT noise program and input values of b and C_{max} (ie. b = 2.5 min^{-1} and C_{max} = 33%). Lastly, the Kety equation was refit to the noisy data set using the values of b and C_{max} generated in the first step. The entire procedure

was repeated 1000 times for each magnitude of tissue buildup CT noise.

Simulations were run using a scanning protocol of 1 baseline scan and 6 enhanced scans, each separated by 1 minute [Bews et al, 90], a slight modification to the one used in the previous sections. Studies were carried out for both grey and white matter and over a range of CT noise: (0 to 1.5 HU standard deviation). In the case of the white matter simulations for noise greater than 1.0 HU, it was necessary, for statistical reasons, to increase the number of runs from 1000 to 5000.

Results

The uncertainty associated with grey matter flow measurements, due to CT noise in the tissue buildup images alone and CT noise combined with the expired air scanning technique is illustrated in figure 19(a). The solid lines represent the 5 and 95 percentiles from the CT noise simulations and the dashed lines represent the corresponding percentiles from the simulations of the expired air scanning technique combined with CT noise. The uncertainty in white matter flow measurements is illustrated in figure 19(b).

Figure 19

The uncertainty in flow measurements due to CT noise in the head images and the implementation of the expired air scanning technique for (a) grey matter and (b) white matter. The 5 and 95 percentiles from the CT noise simulations are presented by the dased lines. The percentiles from the simulations combining the effects of CT noise and the expired air scanning technique are represented by the solid lines. The input value is represented by the dotted line.

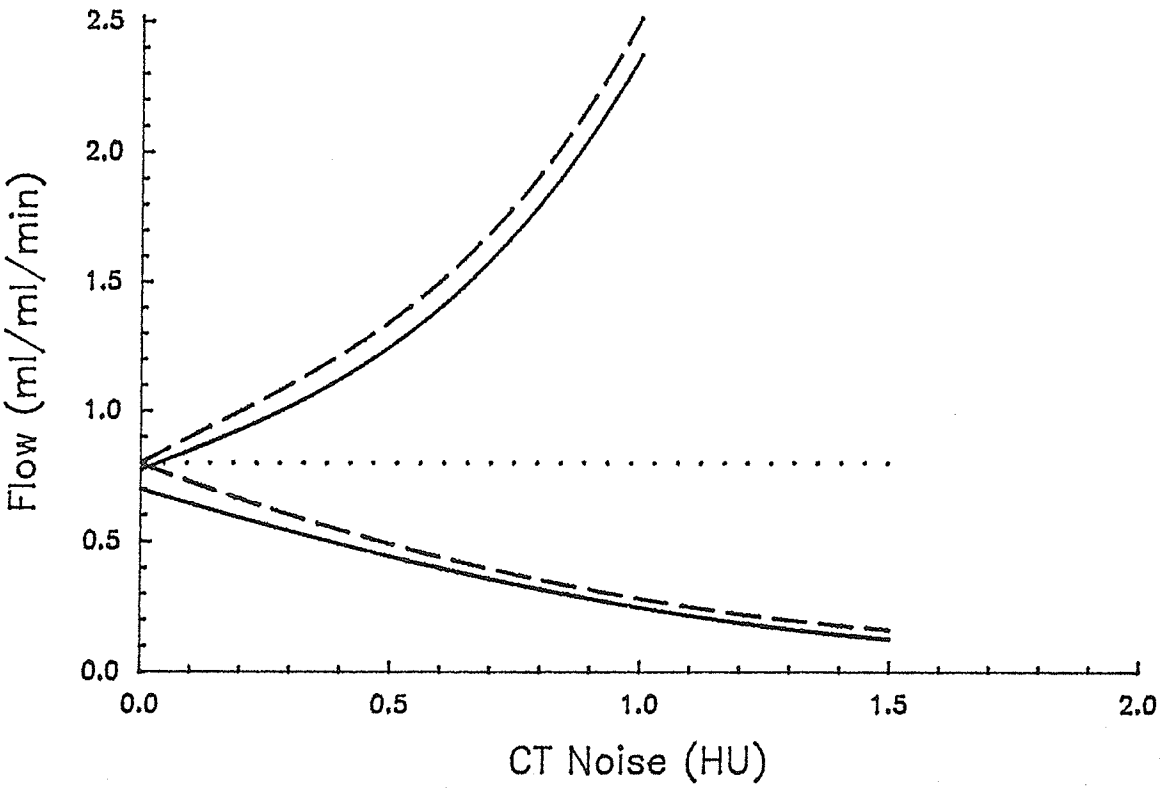
2.5
2.0
1.5
1.0
0.5
0.0
Flow (ml/ml/min)
0.0
0.5
1.0
1.5
2.0
CT Noise (HU)

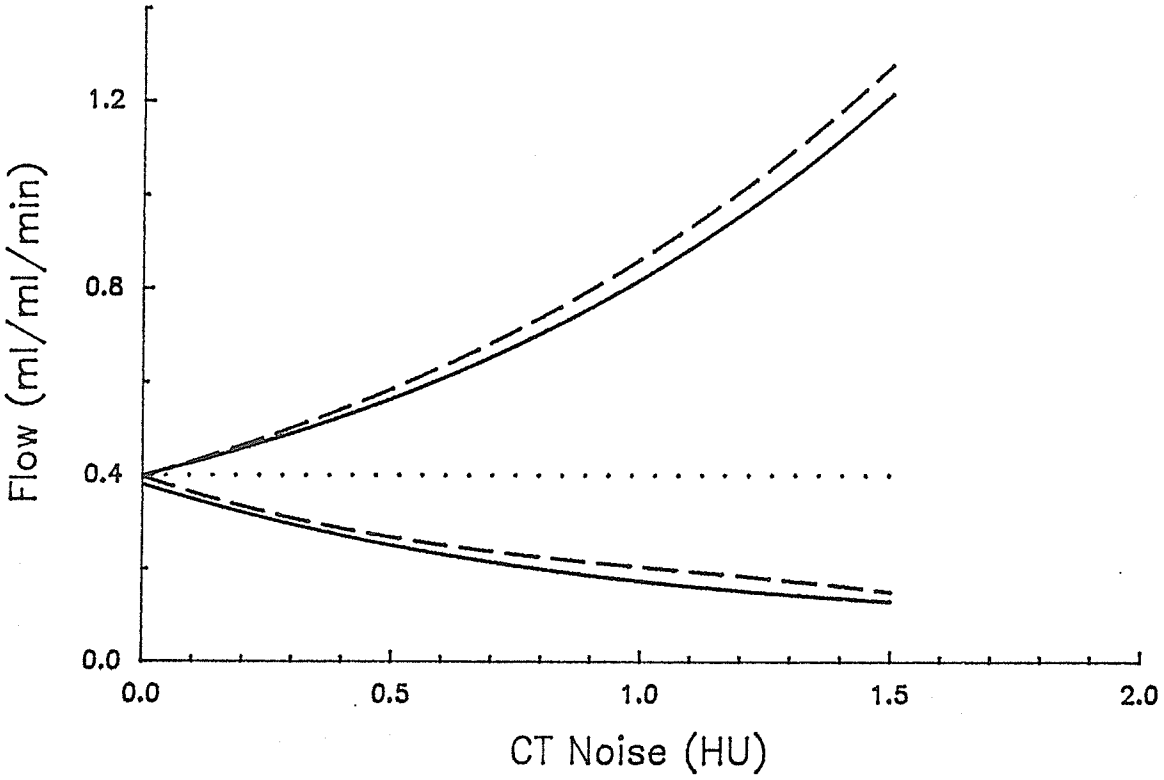
1.2
0.8
0.4
0.0
Flow (ml/ml/min)
0.0
0.5
1.0
1.5
2.0
CT Noise (HU)

Discussion

At the CT noise level of 0, the 5 and 95 percentiles from the CT noise simulations are equal to the input value, as expected. The corresponding percentiles from the simulations of the expired air scanning technique combined with CT noise, meanwhile, do not converge to the input value. In fact, in the absence of noise, both the 5 and 95 percentiles fall below the input value. This bias is due to the relationship between the error in the breathing curve rate constant b and the corresponding error in rCBF. As discussed in section 4.4, the expired air scanning technique results in b being overestimated. It has been determined that if b is overestimated, the corresponding value of rCBF will be underestimated [Good et al, 81a]. In the presence of CT noise, this over estimation of b results in a downward shift in the flow distribution.

It is evident by comparing the spread of the flow distributions that errors in rCBF measurements introduced by the expired air scanning technique are relatively insignificant compared to errors due to CT noise. It is only for extremely small values of CT noise (ie. less than 0.1 HU) that errors due to the scanning technique are significant. Generally, the only noticeable result of using the expired air scanning technique is a minor loss of accuracy.

Although the results were not shown, these simluations were run with a breathing curve rate constant equal to 1.5 and 3.5 min^{-1} in addition to a value of 2.5. These simulations were performed to determine if the magnitude of the error in rCBF due to the implimentation of the expired air scanning technique would

change significantly with different values of the breathing curve rate constant. It was determined that the magnitude of this error changed little compared to the error due to CT head noise, when different values of the breathing curve rate constant were used.

4.6 Conclusions

The feasibility of the expired air scanning technique was investigated in this chapter with the aid of computer simulations and phantom measurements. The following conclusions were reached:

1) The CT scanner used in this study (GE9800) possesses the sensitivity to detect changes in the concentration of xenon in air found in a typical XeCT clinical study. Furthermore, it was discovered that the relationship between CT number and xenon concentration in air is linear thereby making this technique self-calibrating.

2) The duration of a CT scan will greatly affect rCBF measurements. Generally, increasing the scan duration, will result in more precise rCBF measurements, howver at the expence of accuracy.

3) The error in rCBF measurements due to the transit volume is quite small. To ensure that this error is minimized, the length of the tube extending from the patient's mouth to the scan field should be as short as possible.

4) CT noise in the expired air tube images will have little effect on the accuracy of flow estimates, provided the magnitude of the noise falls within the range studied in section 4.4.3. A tube with a diameter of about 2 cm should prove adequate for ensuring the noise is less than 0.2 HU and therefore insignificant.

5) The accurate determination of the breathing curve rate constant b, requires that the rise of the breathing curve be adequately sampled. To satisfy this criterion, a number of scans should be obtained in the first minute of xenon inhalation.

6) The loss of precision and accuracy in flow measurements due to the implementation of the expired air scanning technique is insignificant compared to errors arising from noise in the head images. It is only in situations where the CT noise is quite small (ie. less that 0.1 HU) that the error due to expired air scanning technique becomes significant.

7) Clinical studies of the proposed expired air scanning technique would prove useful for validating its potential benefits, that is, greatly simplifying the application of the XeCT technique with only a small reduction in the overall accuracy and precision.

Chapter 5

Conclusion

Xenon enhanced computed tomography (XeCT) can be used to measure regional cerebral blood flow (rCBF). Two aspects of XeCT were investigated in this study: a comparison of its precision to that of another technique for measuring rCBF and a proposed simplification to its clinical application.

Positron Emission Tomography (PET) is generally considered the best imaging modality for measuring cerebral blood flow and metabolism. To determine how CT compares as an alternative, XeCT was compared to the $C^{15}O_2$ buildup/dynamic PET technique ($C^{15}O_2$PET), which was chosen for this study because of its remarkable similarity to XeCT. The two techniques were compared using Monte Carlo computer simulations to analyze the magnitude of errors introduced into their respective flow measurements by statistical noise (generally considered to be the greatest source of error in both applications). The results of these simulations showed XeCT to yield more precise flow estimates, this being attributed to the better signal to noise ratio associated with CT images compared to PET images.

The second aspect of the XeCT technique investigated was a proposed simplification to its clinical application. The XeCT technique requires measuring the xenon concentration in end-tidal expired air, usually with a thermoconductivity analyzer, as the patient continuously inhales the tracer. The proposed alteration uses the CT scanner to measure the expired air concentration of xenon in conjunction with buildup of tracer in tissue, thus eliminating the need for specialized instruments. In order for this method to be successful, the CT

scanner must be able to measure the concentration of xenon in expired air. Using phantom studies, it was verified that the CT scanner does have this capability, and furthermore, it was found that the method is self-calibrating. Computer simulations were used to investigate the possible effect of using this alteration on the accuracy and precision of the flow measurements generated by XeCT. It was determined that this method introduces a bias in flow measurements but has little effect on the precision of flow measurements. To judge the magnitude of the errors due to the expired air scanning technique relative to other potential sources of error in XeCT, the former was compared to the error introduced by the statistical noise in the CT images used to characterize the buildup of xenon in cerebral tissue. This comparison was preformed using Monte Carlo type simulations, and it was determined that the magnitude of the errror due to the expired air scanning technique was considerably smaller that the error introduced by the statistical noise in the tissue buildup images.

References

Alpert NM, Eriksson L, Chang JY, Bergstrom M, Litton JE, Correia JA, Bohm C, Ackerman RH and Taveras JM (1984) Strategy for the Measurement of Regional Cerebral Blood Flow Using Short-Lived Tracers and Emission Tomography. J Cereb Blood Flow Metab. 4:28-34

Barrett HH, and Swindell W (1981) Radiological Imaging: The Theory of Image Formation, Detection and Processing. Chapter 7 and 10. Academic Press, New York

Bews J, Dunscombe PB, Lee TY, McClarty B, and Kroeker MA (1990) The role of noise in the measurement of cerebral blood flow and the partition coefficient using xenon-enhanced computed tomography. Phys Med Biol. 7:937-945

Budinger TF, Derenzo SE, Gullberg GT, Greenberg WL and Huesman RH (1977) Emission Computer Assisted Tomography with Single-Photon and Positron Annihilation Photon Emitters J Comp Assist Tomo. 1:131-145

Budinger TF, Derenzo SE, Greenberg WL, Gullberg GT and Huesman RH (1978) Quantitative Potentials of Dynamic Emission Computed Tomography. J Nucl Med. 19:309-315

Celsis P, Goldman T, Henriksen L, and Lassen NA (1981) A Method for Calculating Regional Cerebral Blood Flow From Emission Computed Tomography of Inert Gas Concentrations. J Comput Assist Tomogr. 5:641-645

Derenzo SE, Zaklad H and Budinger TF (1975) Analytical Study of a High-Resolution Positron Ring Detector System For Transaxial Reconstruction Tomography. J Nucl Med 12:1166-1172

Deshmukh VD and Meyer JS (1978) Noninvasive Measurement of Regional Cerebral Blood Flow in Man. Chapter 8. SP Medical and Scientific Books, New York

Dhawan V, Conti J, Mernyk M, Jarden JO, and Rottenberg DA (1986) Accuracy of PET RCBF Measurements: Effect of Time Shift Between Blood and Brain Radioactivity Curves. Phys Med Biol 5:507-514

Drayer BP, Gur D, Wolfson SK and Cook EE (1980) Experimental Xenon Enhancement with CT Imaging: Cerebral Applications. AJR. 134:39-44

Eichling JO, Raichle ME, Grubb RL and Ter-Pogossian MM (1974) Evidence of

the Limitations of Water as a Freely Diffusible Tracer in Brain of the Rhesus Monkey. Circ Res 35:358-364

Eleff SM, Schnall MD and Ligetti L (1988) Concurrent Measurements of Cerebral Blood Flow Sodium Lactate, and High-Energy Phosphate Metabolism using ^{19}F, ^{23}Na, ^{1}H and ^{31}P Nuclear Magnetic Resonance Spectroscopy. Mag Res Med 7:412-424

Fatouros PP, Wist AO, Kishore PRS, DeWitt DS, Hall JA, Keenan RL, Stewart LM, Marmarou A, Choi SC, and Kontos HA (1987) Xenon/Computed Tomography Cerebral Blood Flow Measurements Method and Accuracy. Invest Radio 9:705-712

Fazio f, Fieschi C, Collice M, Nardini M, Banfi F, Possa M and Spinelli F (1980) Tomographic Assessment of Cerebral Perfusion Using a Single Photon Emitter (Krypton-81m) and a Rotating Gamma Camera. J Nucl Med. 21:1139-1145

Foley WD, Haughton VM, Schimidt J, and Wilson CR (1978) Xenon Contrast Enhancement in Computed Body Tomography. Radiology 129:219-220

Frackowiak RSJ, Lenzi G-L, Jones T and Heather JD (1980) Quantitative Measurement of Regional Cerebral Blood Flow and Oxygen Metabolism in Man Using ^{15}O and Positron Emission Tomography: Theory, Procedure, and Normal Values. J Comput Assist Tomogr. 6:727-736

Gambhir SS, Huang SC, Hawkins RA and Phelps ME (1987) A Study of the Single Compartment Tracer Kinetic Model for the Measurement of Local Cerebral Blood Flow using ^{15}O-Water and Positron Emission Tomography. J Cereb Blood Flow Metab 7:13-20

Good WF, Gur D, Yonas H, and Herron JM (1987) Errors in Cerebral Blood Flow Determinations by Xenon-Enhanced Computed Tomography due to Estimation of Arterial Xenon Concentrations. Med Phys. 14(3):377-381

Good WF and Gur D (1987) The Effect of Computed Tomography Noise and Tissue Heterogeneity on Cerebral Blood Flow Determination by Xenon-Enhanced Computed Tomography. Med Phys. 14(4):557-561

Green JH (1970) An Introduction to Human Physiology. Chapter 5. Oxford University Press, London

Gur D, Wolfson SK, Yonas H, Good WF, Shabason L, Latchaw RE, Miller DM, and Cook BS (1982) Progress in Cerebrovascular Disease: Local Cerebral Blood Flow by Xenon Enhanced CT. Stroke 6:750-758

Gur D, Herron JM, Molter BS, Good BC, Albright RE, Miller JN and Drayer BP (1984) Simultaneous Mass Spectrometry and Thermoconductivity Measurements of End-Tidal Xenon Concentrations: A Comparison. Med Phys. 11(2):209-212

Gur D, Yonas H, Jackson DL, Wolfson SK, Rockette H, Good WF, Maitz GS, Cook EE and Arena VC (1985) Measurement of Cerebral Blood Flow During Xenon Inhalation as Measured by the Microspheres Method. Stroke 5:871-874

Hanson KM (1979) Detectability in Computed Tomographic Images. Med Phys. 6(5):441-451

Herscovitch P, Markham J, and Raichle ME (1983) Brain Blood Measured with Intravenous $H_2{}^{15}O$. I. Theory and Error Analysis. J Nucl Med. 24:782-789

Herscovitch P and Raichle ME (1984) What is the Correct Value for the Brain-Blood Partition Coefficient for Water? J Cereb Blood Flow Metab. 5:65-69

Huda W, Lentle B, and Sutherland JB (1989) The Effective Dose Equivalent in Radiology. J Can Assoc Radiol. 40:3-4

Huda W, Sandison GA, and Lee T (1989) Patient Doses From Computed Tomography in Manitoba From 1977 to 1987. Brit J Rad. 62:138-144

Huda W and Sandison GA (1990) Estimates of the Effective Dose Equivalent, H_E, in Positron Emission Tomography Studies. Eur J Nucl Med. 16 (in press)

Huesman RH (1977) The Effects of a Finite Number of Projection Angles and Finite Lateral Sampling of Projections on the Propagation of Statistical Errors in Transverse Section Reconstruction. Phys Med Biol. 3:511-521

Iida H, Kanno I, Miura S, Murakami M, Takahashi K and Uemura K (1986) Error Analysis of a Quantitative Cerebral Blood Flow Measurement Using $H_2{}^{15}O$ Autoradiography and Positron Emission Tomography, With Respect to the Dispersion of the Input Function. J Cereb Blood Flow Metab. 6:536-545

Junck L, Dhawan V, Thaler HT, and Rottenberg DA (1985) Effects of Xenon and

Krypton on Regional Cerebral Blood Flow in the Rat. J Cereb Blood Flow Metabol. 5:126-132

Kanno I and Lassen NA (1979) Two Methods for Calculation of Regional Cerebral Blood Flow from Emission Computed Tomography of Inert Gas Concentration. J Comput Assist Tomogr. 3:71-89

Kanno I, Lammertsma AA, Heather JD, Gibbs JM, Rhodes CG, Clark JC, and Jones T (1984) Measurement of Cerebral Blood FLow Using Bolus Inhalation of $C^{15}O_2$ and Positron Emission Tomography: Description of the Method and its Comparison with the $C^{15}O_2$ Continuous Inhalation Method. J Cereb Blood Flow Metab. 4:224-234

Kelcz F, Hilal SK, Hartwell P and Joseph PM (1978) Computed Tomographic Measurement of the Xenon Brain-Blood Partition Coefficient and Implications for Regional Cerebral Blood Flow: A Preliminary Report. Radiology 127:385-392

Kearfott KJ, Lu HC and Rottenberg DA (1984) The Effects of CT Drift on Xenon/CT Measurements of Regional Cerebral Blood Flow. Med Phys. 11(5):686-689

Kety SS, and Schmidt CF (1948) The Nitrous Oxide Method for the Quantitative Determination of Cerebral Blood Flow in Man: Theory, Procedure and Normal Values. J Clin Invest. 27:476-484

Kety SS (1951) The Theory and Applications of the Exchange of Inert Gas at the Lungs and Tissues. Pharm Rev. 3:1-41

Kety SS (1985) Regional Cerebral Blood Flow: Estimation by Means of Nonmetabolized Diffusible Tracers - An Overview. Sem Nucl Med. 4:324-328

Kim SG, and Acherman JJH (1988) Mulitcompartment Analysis of Blood Flow and Tissue Perfusion Employing D_2O as a Freely diffusible Tracer: A Novel Deuterium NMR Technique Demonstrated via Application with Murine RIF-1 Tumours. Mag Res Med. 8:410-426

Kishore PRS, Roa GU, Fernandez RE, Keenan RL, Arora GD, Gadisseux P, Stewart LM, Wist AO, Fatouros PP, Dillard D, and Watson CK (1984) Regional Cerebral Blood Flow Measurements Using Stable Xenon Enhanced Computed Tomography: A Theoretical And Experimental Evaluation. J Comput Assist Tomogr. 4:619-630

Koeppe RA, Holden JE, and Ip WR (1985) Performance Comparison of Parameter Estimation Techniques for the Quantification of Local Cerebral Blood Flow by Dynamic Positron Computed Tomography. J Cereb Blood Flow Metab. 5:224-234

Lammertsma AA, Jones T, Frackowiak RSJ, and Lenzi GL (1981) A Theoretical Study of the Steady-State Model for Measuring Regional Cerebral Blood Flow and Oxygen Utilization Using Oxygen-15. J Comput Assist Tomogr 4:544-550

Lammertsma AA, Wise RJS, Cox TCS, Thomas DGT and Jones T (1985) Measurement of blood flow, oxygen utilization, oxygen extraction ratio and fractional blood volume in human brain tumours and surrounding edematous tissue. Brit J Rad. 58:725-734

Lammertsma AA, Frackowiak RSJ, Hoffman JM, Huang S-C, Weinberg IN, Dahlbom M, MacDonald NS, Hoffman EJ, Mazziotta JC, Heather JD, Forse GR, Phelps ME, and Jones T (1989) The $C^{15}O_2$ Build-up Technique to Measure Regional Cerebral Blood Flow and Volume of Distribution of Water. J Cereb Blood Flow Metab. 9:461-470

Lassen NA, and Munck O (1954) The Cerebral Blood Flow in Man Determined

by the Use of Radioactive Krypton. Acta phys. Scandinav. 33:30-49

Lassen NA and Klee A (1964) Cerebral Blood Flow Determined by Saturation and Desaturation with Krypton. Circ Res. 16:26-33

Lassen NA, Sveinsdottir E, Kanno E, Stokely M and Rommer P (1968) A Fast Moving Single Photon Emission Tomograph for Regional Cerebral Blood Flow Studies in Man. J Comput Assist Tomogr. 2:661-672

Lassen NA (1985) Cerebral Blood Flow Tomography with Xenon-133. Sem Nucl Med. 14:347-355

Lee TY, Ellis RJ, Dunscombe PB, McClarty B, Hodson DI, Kroeker MA, and Bews J (1990) Quantitative Computed Tomography of the brain with Xenon Enhancement: A Phantom Study with the GE9800 Scanner. Phys Med Biol. 7:925-935

Lee TY (1990) Private Communication

Majumdar S, Zoghbi S, Pope CF, Gore JC (1989) A Quantitative Study of Relaxation Rate Enhancement Produced by Iron Oxide Particles in Polyacrylamide Gels and Tissue. Mag Res Med 9:185-202

McHenry LC (1978) Cerebral Circulation and Stroke. Chapter 4. Warren H. Green Inc., St. Louis

Meyer JS, Hayman LA, Amano T, Nakajima S, haw T, Lauzon P, Derman S, Karacan I, and Harati Y (1981) Mapping Local Blood Flow of Human Brain by CT Scanning During Stable Xenon Inhalation. Stroke 4:426-436

Miller DD, Holmvang G, Gill JB, et al (1989) MRI Detection of Myocardial Perfusion Changes by Gd-DTPA Infusion during Dipyridamole Hyperaemia. Mag Res Med. 10:246-255

Nelson DF, Urtasun RC, Saunders WM, Gutin PH, and Sheline GE (1986) Recent and Current Investigations of Radiation Therapy of Malignant Gliomas" Sem in Oncology 13:46-55

Obrist WD, Thompson HK, King H and Wang HS (1967) "Determination of Regional Cerebral Blood Flow by Inhalation of 133-Xenon. Circ Res. 20:124-135

Obrist WD, Thompson HK, Wang HS and Wilkinson WE (1975) Regional Cerebral Blood Flow Estimated by ^{133}Xenon Inhalation. Stroke. 6:245-

256

Ott RJ (1989) Nuclear medicine in the 1990s: A Quantitative Physiological Approach. Brit J Rad. 62:421-432

Raichle ME, Martin WRW, Herscovitch P, Mintun MA and Markham J (1983) Brain Blood Flow Measured with Intravenous $H_2{}^{15}O$. II. Implementation and Validation. J Nucl Med. 24:790-798

Riederer SJ, Pelc NJ and Chesler DA (1978) The Noise Power Spectrum in Computed X-ray Tomography. Phys Med Biol. 3:446-454

Rescigno A and Boicelli A (1988) Cerebral Blood Flow: Mathematical Models, Instrumentation and Imaging Techniques. Chapter 3. Plenum Press, New York

Rottenberg DA, Lu HC and Kearfott KJ (1982) The In Vivo Autoradiographic Measurement of Regional Cerebral Blood Flow Using Stable Xenon and Computerized Tomography: The Effect of Tissue Heterogeneity and Computerized Tomography Noise. J Cereb Blood Flow Metab. 2:173-178

Shapiro WR, and Shapiro JR (1986) Principles of Brain Tumour Chemotherapy. Sem in Oncology 13:56-69

Subramnyam R, Alpert NM, Hoop B, Brownell GL and Taveras JM (1978) A Model for Regional Cerebral Oxygen Distribution During Continuous Inhalation of $^{15}O_2$, C^{15}O and $^{15}O_2$. J Nucl Med 19:48-53

Taylor DG, Inamdar R and Bushell MC (1988) NMR Imaging in theory and in practice. Phys Med Biol 6:636-670

Ter-Pogossian MM (1981) Special Characteristics and Potential for Dynamic Function Studies with PET. Semin Nucl Med 1:13-23

Veall N, Mallett BL (1965) The Partition of Trace Amounts of Xenon between Human blood and Brain Tissues at 37°C. Phys Med Biol 10:375-380

Webb S (1988) The Physics of Medical Imaging. Chapter 4 and 8. IOP Publishing Ltd. Bristol

Weinberg IN, Huang SC, Hoffman EJ, Araujo L, Nienaber C, Grover-McKay M and Schelbert H (1988) Validation of PET-Acquired Input Functions for Cardiac Studies. J Nucl Med 29:241-247

Yonas H, Wolfson SK, Gur D, Latchaw RE, Good WF, Leanza R, Jackson DL, Jannetta PJ, and Reinmuth OM (1984) Clinical Experience with the Use of Xenon-Enhanced CT Blood Flow Mapping in Cerebral Vascular Disease. Stroke 3:443-450

Yonas H, Gur D, Good WF, Maitz GS, Wolfson SK and Latchaw RE (1985) Effects of Xenon Inhalation on Cerebral Blood Flow: Relevance to Humans of Reported Effects in the Rat. J Cereb Blood Flow Metab 4:613-614

Appendix I: **Noise in reconstructed images**

A primary source of noise in a reconstructed image is the statistical fluctuations in the detected photons. Extensive research has been carried out on the relationship between the uncertainty in a reconstruction and this quantum noise [Budinger et al, 77; Riederer et al, 78; Hanson, 79; Huesman, 77] . One result of this research is the following simple formula describing the signal-to-noise ratio in a reconstructed image [Budinger et al, 77]:

$$\frac{signal}{noise} = \frac{(total\ number\ of\ detected\ events)^{1/2}}{1.2\ (total\ number\ of\ pixels)^{3/4}} \qquad (23)$$

The object of this appendix is to outline the derivation of this formula.

The reconstruction algorithm considered in this outline is filtered back-projection with simple parallel geometry data collection. The noise power spectrum will be used to characterize the statistical noise in the image.

Let $S_p(f_x)$ be the noise power spectrum for a single projection. Each projection is filtered through a corrective filter, $G(f_x)$. If the imaging system is considered linear and shift invariant, the noise power spectrum of a single filtered projection is:

$$S_f(f_x) = S_p(f_x)\,|G(f_x)|^2 \qquad (24)$$

The filtered projection is back-projected in the direction along which it was measured (the y direction). From the definition of back-projection there is no variation of the noise along the y-direction [Riederer et al, 78]. The noise power spectrum of the image, $S_b(f_x,f_y)$, due to a single back-projection can therefore be

written as:

$$S_b(f_x, f_y) = S_p(f_x)\,|G(f_x)|^2\,\delta(f_y) \tag{25}$$

Notice that the noise power spectrum for only one projection contributes to the total noise power spectrum of the image along the spoke $f_y = 0$. Similarly, each additional projection will only contribute to the total power spectrum along a single spoke. Therefore, the total power spectrum is the superposition of the contribution from each projection. If there are M such projections at equally spaced angles from 0 to π, then the spoke density at a frequency f ($f = f_x^2 + f_x^2$) is $M/f\pi$. The total power spectrum of the image is:

$$S(f) = \frac{M}{f\pi}\left[\frac{\pi}{M}\right]^2 |G(f)|^2 S_p(f) \tag{26}$$

where $M/f\pi$ is a normalization constant for the reconstruction [Riederer et al, 78].

The noise variance in the reconstruction image is given by [Hanson, 79]:

$$\sigma_I^2 = \int_{-\infty}^{\infty}\int_{-\infty}^{\infty} df_x df_y\; S(f_x, f_y) \tag{27}$$

$$\sigma_I^2 = \int_0^{2\pi}\int_0^{\infty} fS(f)\, df d\phi \tag{28}$$

$$\sigma_I^2 = \frac{\pi}{M}\int_0^{2\pi}\int_0^{\infty} S_p(f)\,|G(f)|^2 df \tag{29}$$

If the projection data are obtained from equally spaced, uncorrelated measurements and all the measurments in a projection have identical means, then

the noise power spectrum of one projection is [Hanson, 79]:

$$S_p(f) = \begin{cases} \Delta l \sigma_p^2 & |f| \leq 1/2\Delta l \\ 0 & |f| > 1/2\Delta l \end{cases} \qquad (30)$$

where Δl is the spacing between the projection measurements whose variance is σ_p^2. The variance in the reconstructed image becomes:

$$\sigma_I^2 = 2\frac{\pi^2}{M}\sigma_p^2 \int_0^{\frac{1}{2\Delta l}} |G(f)|^2 df \qquad (31)$$

To obtain an expression for the noise variance, a filter function, G(f) must be chosen. For the Hanning filter:

$$G(f) = \begin{cases} \frac{1}{2}f[1+\cos(\pi f/f_c)] & f \leq f_c \\ 0 & \text{otherwise} \end{cases} \qquad (32)$$

where $f_c = 1/2\Delta l$.

The corresponding noise variance is:

$$\sigma_I^2 = \sigma_p^2\left[\frac{0.07}{\Delta l^2 M}\right] \qquad (33)$$

If the object being reconstructed is circular with a diameter D, and has uniform concentration of activity, then the relationship between the projection p_i and the activity concentration I_j in the j^{th} cell is [Huesman, 77]

$$p_i = \sum_{j=1}^{v} \Omega_{ij} I_j \qquad (34)$$

where Ω_{ij} is the line length of the i^{th} path through the j^{th} cell, v is the total number

of cells and is equal to $(\pi/4)(D/d)^2$ and d is the pixel length. The average projection value for the circular reconstruction region is found from equation (34) to be:

$$\langle p \rangle = \frac{\pi D}{4} \langle I \rangle \tag{35}$$

The total number of projections is given by:

$$n_T = \frac{D}{\Delta l} M \tag{36}$$

Using the equations (33),(35) and (36) the noise-to-signal ratio can be written as:

$$\frac{\sigma_I}{\langle I \rangle} = \sigma_p \left[\frac{0.07D}{\Delta l^3 n_T} \right]^{\frac{1}{2}} \frac{\pi D}{4 \langle p \rangle} \tag{37}$$

The sampling interval between projections Δl, must be of the order of (0.4 - 0.7) of the pixel size d, to satisfy the condition of adequate sampling [Huesman, 77]. The total number of detected events is $n_T\langle p \rangle$ and, as stated before, the total number of cells is $(\pi/4)(D/d)^2$. Due to the Poisson nature of the emitted photons, $\sigma_p^2 \approx \langle p \rangle$. Combining all of these statements, the noise-to-signal ratio can be written as:

$$\frac{noise}{signal} = \frac{1.2\,(total\ number\ of\ pixels)^{\frac{3}{4}}}{(total\ number\ of\ detected\ events)^{\frac{1}{2}}} \tag{38}$$

Using equation (38), the noise in a reconstructed image can be estimated.

Appendix II: Signal-to-Noise Calculations (SNR)

All calculations are for grey matter and a 2.0 cm^2 region of interest.

A) XeCT Simulations

The enhancement in CT number for the serial CT images were calculated using equation (15) on page 22 and the noise using equation (17) on page 39.

Time (min)	Enhancement (HU)	Noise (HU)	SNR
1	2.38	0.17	14
2	4.19	0.17	25
3	4.94	0.17	29
4	5.22	0.17	31
5	5.32	0.17	31
6	5.38	0.17	32

B) $C^{15}O_2$PET Simulations

The SNR results are presented for an inhaled $C^{15}O_2$ concentration of 20 μCi/ml. The average signal per pixel was determined using equation (19) (page 40), assuming a 20 cm diameter head and a pixel dimension of 0.5 cm. The noise was calculated using equation (20) (page 41) to determine the variance in a pixel and equation (17) (page 39) to determine the standard error in a ROI.

Time (min)	Duration (sec)	Signal (cts)	Noise (cts)	SNR
1	10	123	28	4
2	20	474	55	9
3	20	560	58	10
4	20	656	65	10
5	30	1002	80	13
6	30	1035	81	13

C) **$C^{15}O_2$PET Simulations**

SNR results are presented for an inhaled $C^{15}O_2$ concentration of 30 μCi/ml.

Time (min)	Duration (sec)	Signal (cts)	Noise (cts)	SNR
1	10	184	34	5
2	20	712	67	11
3	20	900	76	12
4	20	984	79	12
5	30	1527	99	15
6	30	1553	100	16

Appendix III: **Computer Simulations**

Errors introduced into rCBF measurements as a result of the expired air scanning technique, were investigated using computer simulations. The computer program used in this study can be separated into two parts. The first quantifies the errors in characterizing the breathing curve by the expired air scanning technique while the second examines the effect of these errors on the accuracy and precision of rCBF measurements.

The first part of the program simulates the time course of xenon flowing through the expired air tube using a sinusoidal function:

$$C(t) = C_{max}\left[\begin{array}{l} 1 + \frac{1}{2}e^{-bt}\sin(2\pi wt - \frac{\pi}{2}) - \frac{1}{2}e^{-bt} \\ \quad + Ae^{-bt} - Ae^{-bt}\sin(2\pi wt + \frac{\pi}{2}) \end{array}\right] \qquad (39)$$

where C(t) is the concentration of xenon in air at a time t, w is the breathing frequency (breaths/min) and A is an amplitude factor introduced to take into account deadspace (ie. the volume of air that enters the body but does not reach the lungs [Green, 70]). It has been estimated that approximately three eighths of a resting person's breath is dead space. In this program, A is chosen so as to force the function through C_{max} at three eighths of a breath. The computer program then restricts the function to values less than or equal to C_{max}, thereby creating a dead space plateau at the beginning of each exhalation.

The time course of the concentration of xenon in the expired air tube can be divided into two parts. During the exhalation portion of the patient's breathing cycle, expired air flows through the tube and can be represented by the

above function. Conversely, during inhalation, the gas in the tube is static and the xenon concentration in the tube is described by a constant value, which depends entirely on the length of time the patient has been inhaling xenon. The computer simulated time course of xenon in the expired air tube is shown in Figure 20. The plateaus at C_{max} at the beginning of every exhalation corresponds to dead space and the troughs following each end tidal point represent the static portion of the breathing cycle (ie. inhalation).

At rest, a person's breathing frequency varies between fifteen and twenty breaths per minute with approximately 400 ml of air inhaled with every breath [Green, 70]. For this study an initial breathing frequency of 17.5 breaths/minute was adopted and every breath was assumed to contain 400 ml of air.

Initial applications of this simulation revealed a design problem that was traced back to the use of a constant breathing frequency to calculate the concentration of xenon in the expired air tube. It became evident that the phase coherence between this frequency and the frequency of the scans played a significant role in determining the magnitude of error in the derived values of b. This phase coherence however does not exist in the clinical situation for a patient is not expected to maintain the same breathing frequency over the entire duration of the study. Unfortunately, simulating the actual breathing pattern of a patient would be very difficult. A patient could increase or decrease his breathing rate at any moment, or pause any numerous times during the study. Instead of attempting to simulate these fluctuations, a simpler method was adopted in which

Figure 20

The computer simulated time course of xenon in the expired air tube (solid line). The plateaus at the end-tidal concentration curve represent the static air in the tube as the patient inhales. The falls of the curve represent the concentration of xenon in the tube as the patient exhales.

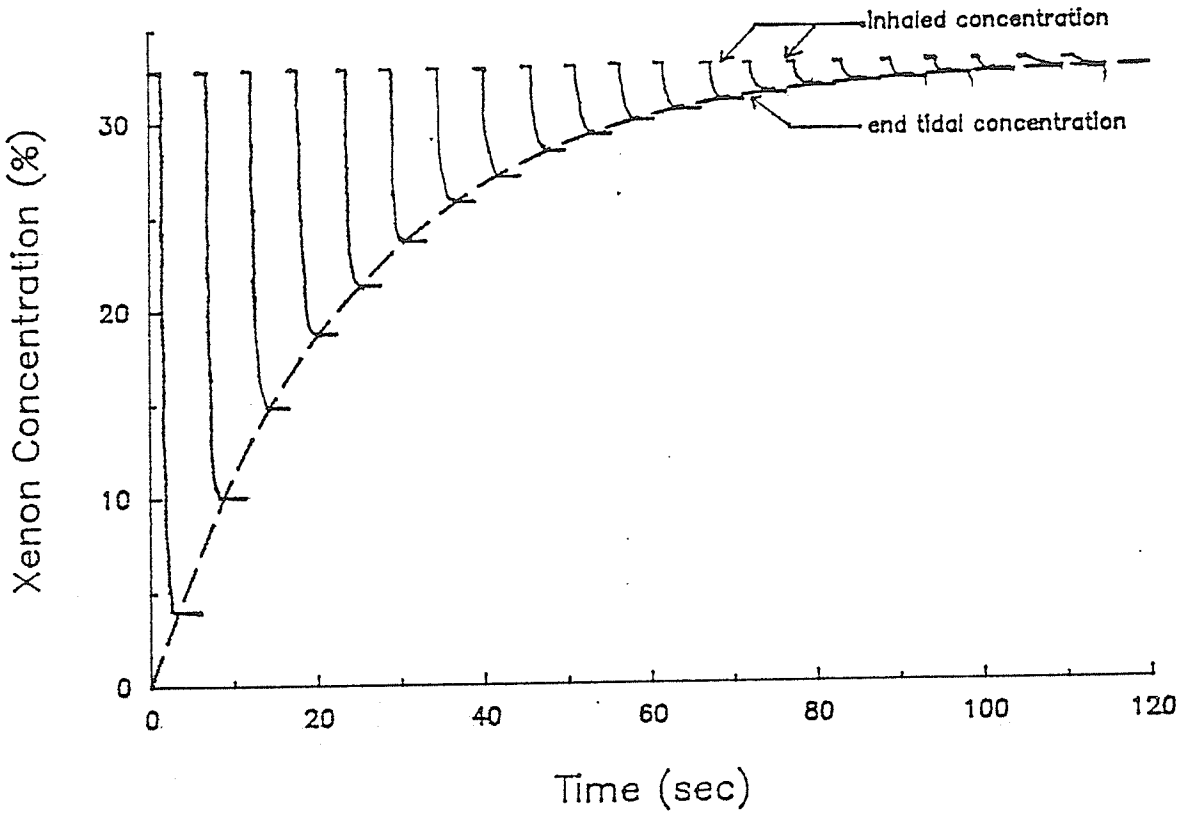
Inhaled concentration
end tidal concentration
Xenon Concentration (%)
0
10
20
30
0
20
40
60
80
100
120
Time (sec)

a random number generator altered the breathing frequency between 17.5 and 19.5 breaths/minute before each CT scan. This refinement eliminates the constant phase relationship and leads to more realistic results.

Inaccuracies in b and C_{max} occur due to the inability of the expired air scanning technique to measure the end tidal xenon concentration in expired air at each sampling time. Sampling of the breathing curve using the CT scanner will be random in nature due to variations in the patient's breathing frequency and as such, the computer simulation must be run numerous times to cover all possible events. The distribution of b resulting from the repeated simulations serve to quantify the precision and accuracy of the proposed technique.

The second part of the computer simulation was designed to analyze the effect of errors in b and C_{max}, arising as a result of the expired air scanning technique, on the accuracy and precision of rCBF measurements. A curve, representing the buildup of xenon in brain tissue C(t), is generated using the Kety equation in conjunction with theoretical values of b, C_{max}, k and λ. The Kety equation is then refit to the tissue buildup data points (sampled from this curve) using the values of b and C_{max} generated in the first part of the computer simulation to yield best fit estimates of k and λ in the presence of expired air scanning errors. rCBF is the product of these two parameters.